1980

Bonding in scandium monosulfide a NaCl crystal type

Jean Ann Merrick
Iowa State University

MERRICK, JEAN ANN

BONDING IN SCANDIUM-MONOSULFIDE A SODIUM-CHLORIDE CRYSTAL TYPE

Iowa State University PH.D. 1980

PLEASE NOTE:

In all cases this material has been filmed in the best possible way from the available copy. Problems encountered with this document have been identified here with a check mark ✓.

1. Glossy photographs _____
2. Colored illustrations _____
3. Photographs with dark background _____
4. Illustrations are poor copy _____
5. Print shows through as there is text on both sides of page _____
6. Indistinct, broken or small print on several pages _____ throughout _____
7. Tightly bound copy with print lost in spine _____
8. Computer printout pages with indistinct print ✓
9. Page(s) _____ lacking when material received, and not available from school or author _____
10. Page(s) _____ seem to be missing in numbering only as text follows _____
11. Poor carbon copy _____
12. Not original copy, several pages with blurred type _____
13. Appendix pages are poor copy _____
14. Original copy with light type _____
15. Curling and wrinkled pages _____
16. Other _____

Bonding in scandium monosulfide a NaCl crystal type

by

Jean Ann Merrick

A Dissertation Submitted to the
Graduate Faculty in Partial Fulfillment of the
Requirements for the Degree of
DOCTOR OF PHILOSOPHY

Department: Chemistry
Major: Physical Chemistry

Approved:

Signature was redacted for privacy.

In Charge of Major Work

Signature was redacted for privacy.

For the Major Department

Signature was redacted for privacy.

For the Graduate College

Iowa State University
Ames, Iowa

1980

TABLE OF CONTENTS

GENERAL INTRODUCTION

Transition metal sulfides exhibit a wide variety of structural and physical properties which have been extensively studied. This class of compounds has been recently reviewed by Jellinek (1) and by Rao and Pisharody (2). As a group, the compounds are refractory, having high melting points and low vapor pressures at high temperatures; most are either semiconductors or metallic conductors, some are superconductors; the magnetic properties range from exhibiting weak diamagnetism to temperature-dependent Pauli paramagnetism; wide homogeneity ranges are observed for some of the sulfides, where ordering of the resultant vacancies may give rise to new phases. The sulfides would be suitable for technological applications as high temperature containers (in nonoxidizing atmospheres), as semiconductors, or as catalysts. The technological prospects of some closely related carbides and nitrides have been discussed by Bennett, et al. (3).

In addition to exploiting the diverse properties of the transition metal compounds, chemists and physicists wish to understand the role of the d electrons, and the nature of the interactions involved in bonding in these compounds. Covalent, ionic, and metallic bonding are all thought to be important.

The inter-relationship between structure and bonding of metal-rich compounds, including the sulfides, has been discussed by Franzen (4). It is found that, whereas most of the one-to-one oxides and nitrides crystallize in the NaCl-type structure, relatively few of the one-to-one sulfides choose the NaCl structure type, preferring instead the NiAs, WC, or MnP type structures. It has been proposed that the increased metal-metal bonding allowed by a NiAs-structure type stabilizes that structure type with respect to the NaCl-structure type, the structure type favored by increased ionicity (4).

The scandium-sulfur system is a representative example of the transition metal sulfides as a group. Several different crystal phases are known (orthorhombic, rhombohedral, fcc) (5); a wide homogeneity range is observed ($Sc_{0.81}S$ to $Sc_{1.00}S$) (6); a phase transition resulting from vacancy ordering occurs in $Sc_{0.81}S$ (6); Sc_2S_3 is a semiconductor, whereas compositions with Sc/S > 0.666 are metallic conductors (7); ScS is also superconducting (8,9); the monosulfides have melting points well above 2000°C (6). Also, ScS is one of the few transition metal monosulfides which crystallizes in the NaCl-type structure. The structures and properties of the phases of the scandium-sulfur system are summarized in Table 1.

Table 1. Structure and properties of phases in the scandium-sulfur system

	Sc_2S_3	$Sc_{1.37}S_2$	$Sc_{0.81}S$[a] ——→	$Sc_{1.00}S$
1. Molar ratio Sc/S	0.666	0.685	0.806 ——→	1.000
2. Color	Yellow	Black	Purple ——→	Gold
3. Structure	Orthorhombic (superstructure of NaCl-type structure; metal vacancies are ordered)	Rhombohedral (superstructure of NaCl-type structure; metal vacancies are partially ordered)	NaCl structure type (partial ordering of vacancies T_{order} = 700°C)	(no vacancies)
4. Space group	Fddd	$R\bar{3}m$	$R\bar{3}m$ at T < 700°C $Fm3m$ at T > 700°C	$Fm3m$
5. Unit cell dimensions	a = 10.41 Å b = 7.38 Å c = 22.05 Å	a = 6.331 Å = 33° 34	a = 5.165 Å ——→	a = 5.190 Å
6. Electrical properties	Semiconductor 2.78 eV band gap	$\rho^b = 3\times10^{-4}$ Ω-cm		$\rho^b = 2\times10^{-5}$ Ω-cm low temperature superconductor T_c = 5.37K
7. Melting point	1775°C		>2000°C congruently vaporizing phase	>2000°C
8. References	5,6	5	6,10	5,6,8,9,10

[a]The arrow denotes a homogeneity range.

[b]Resistivity at 300K.

In addition to the interesting properties observed for the scandium sulfides, the position of Sc itself on the periodic table makes scandium compounds prime candidates for study.

Scandium ((Ar) $3d^1 4s^2$) is a member of the first transition series ((Ar)$3d^n 4s^2$). Compounds formed by members of this series would show trends resulting from increased contributions of d electrons to the valence-conduction band region. Scandium also has the same electronic configuration as the lanthanides ((Xe)$4f^n 5d^1 6s^2$) neglecting the 4f states. In some lanthanide compounds, the 4f electrons occupy states below the valence band and hence would be expected to have properties similar to those of the related scandium compounds. Scandium sulfide also serves to bridge the gap between the ionic alkali metal sulfides, which have no d electrons participating in bonding, and the more covalent transition metal sulfides, whose properties depend largely upon the contributions of the d electrons in metal-metal or metal-nonmetal interactions.

Explanation of the Dissertation Format

The scandium-sulfur system was investigated from the viewpoints of crystal structure, thermodynamics, and electronic structure in an attempt to create a more complete picture of bonding in the material.

Section I of the dissertation describes an attempt to apply a purely ionic model to rationalize the vacancy ordering in $Sc_{0.81}S$. Section II describes a thermodynamic study of ScP which, when compared to a similar study of ScS, allows one to make predictions as to the stabilizing or destabilizing effects of metal-metal bonding in ScS. Section III describes electronic band structure calculations of ScS, which provide details of the bonding interactions taking place in the valence-conduction band region. Section IV describes an X-ray photoelectron spectroscopy study of the various scandium sulfide phases in which measurements were made of the relative shielding or deshielding experienced by electrons throughout the series of compounds. Finally, the results are summarized in an attempt to describe more completely the bonding interactions in scandium sulfide and to extend the description to include other isostructural transition metal materials.

SECTION I. VACANCY ORDERING IN DEFECT SCANDIUM MONOSULFIDE

INTRODUCTION

A number of early transition metal chalcides with an ideal stoichiometry ratio M/X = 1.0 crystallize in the NaCl structure type and have been observed to have wide homogeneity ranges ascribed to vacancies in either the anion or cation sublattice or both. In some cases, vacancy ordering occurs to produce sublattices or superstructures of the original structure. Some examples are TiO (1), NbO (2), ScS (3), and ZrS (4) and LuS (5).

The driving force for the ordering process is not known; however, since the NaCl structure is considered a prototype ionic structure, it has been rationalized by application of the Born-Haber cycle (6,7) and coulombic models to calculate crystal lattice (Madelung) energies. It is the purpose of this work to test the hypothesis that vacancy ordering occurs as a result of coulombic interactions.

The approach developed for this test was to generate a group of ordered vacancy sublattices on the NaCl lattice and to calculate the Madelung energy and configurational entropy contributions for each.

The compound $Sc_{0.8}S$ was chosen from the examples above to test the coulombic model, first, because the ordered superstructure is small (2 times the primitive NaCl cell) and secondly, because Sc is the first of the transition

metals ($4s^2 3d^1$ configuration), and therefore presumably has a relatively small d-orbital contribution to its bonding. To a first approximation, $Sc_{1-x}S$ is assumed to behave in a similar fashion to CaS, an ionic sulfide. The superstructure cell of $Sc_{0.8}S$ has been described (3) as a rock salt structure in which the vacancies occur in alternate metal planes along the body diagonal of a fcc cell (Fig. I.1). Random occupancy within a given plane results in the space group $R\bar{3}m$.

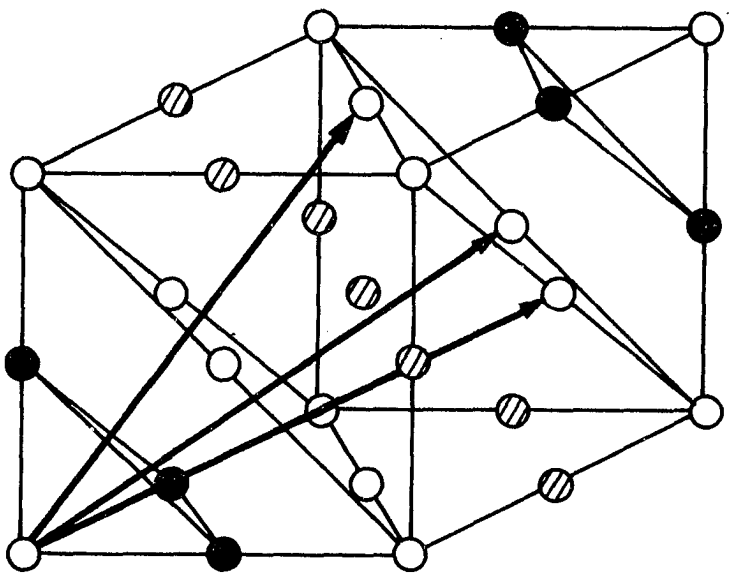

Fig. 1.1. The relationship between the NaCl-type disordered and the $R\bar{3}m$ ordered structures of $Sc_{0.8}S$. Black circles represent Sc sites; hatched circles, partially occupied Sc sites; and open circles, S sites. The $R\bar{3}m$ lattice vectors are indicated.

THEORY AND METHOD

Crystal Lattice Energy

The crystal lattice energy U is typically defined for ionic solids (8,9) as the coulombic energy of interaction between ions on a lattice, where the ions are described as point charges or nonoverlapping, spherically symmetric charge distributions fixed at positions on a regular lattice. The simplest expression for U is

$$U = \frac{1}{2} \sum_{i \neq j} \sum_{j} \frac{q_i q_j}{|\vec{r}_{ij}|} \tag{1.1}$$

where q_i, q_j are the charges associated with the i^{th} and j^{th} ions, respectively, $\vec{r}_{ij}$ is the distance between ions, and the factor of 1/2 corrects for overcounting interactions in the double summation. In some cases, it is convenient to define the total lattice energy in terms of the site potential ϕ_i, the potential felt by a unit charge located at a lattice site.

$$\phi_i = e \sum_{j} \frac{q_i}{|\vec{r}_{ij}|} \tag{1.2}$$

and Eqn. 1.1 becomes

$$U = \sum_{i} q_i \phi_i / 2 \tag{1.3}$$

In 1918, Madelung (10) recognized that the sum over the lattice points could be expressed as a unitless constant, the Madelung constant M, dependent only upon the crystal lattice geometry. The site potential in a crystal of univalent ions in terms of the Madelung constant is

$$\phi_i = - Me^2/r_o \qquad (1.4)$$

where e is the electronic charge and r_o is the shortest anion-cation distance. It should be noted that the definition of the Madelung constant for other than univalent ions is often ambiguous (11).

The expression for the Madelung constant is an infinite alternating series -- a sum of attractive and repulsive terms. An infinite series, which is shown to converge to a limit α, may be equated with α in a mathematical expression, where α is known as the sum of the series. It is the case for a convergent series that a sum of a finite number of terms closely approximates α for that series. The lattice sum described above, however, is conditionally convergent, i.e., the limit depends upon the order of summation (12).

Conditionally convergent sums may be evaluated either by breaking the cell into electronically neutral subcells and evaluating the sum directly, a method credited to Evjen (13), or by the method proposed by Ewald (14), who

expanded the point charge lattice into a periodic Gaussian charge distribution and obtained rapid convergence by proper choice of the Gaussian half-width. The method of Ewald has the advantage that it is more generally applicable to all crystal systems than is the method of Evjen and was the method selected for this study. The application of Ewald's method to the evaluation of lattice sums has been described by Kittel (15) and Tosi (9).

The lattice site potential ϕ_i is defined as the electrostatic potential between a unit point charge located at the i^{th} ion site and the point charges at all other ion sites, with the ion at the i^{th} site removed. Applying Ewald's method to the evaluation of ϕ_i, the lattice is assumed to be constructed in two parts, where the total site potential is the sum of the site potentials of each part

$$\phi_i = \phi_A(i) + \phi_B(i). \tag{1.5}$$

The first component is the potential of a lattice of normalized Gaussian charge distributions centered at each ion site and is expressed as

$$\phi_A(i) = \frac{4\pi}{\Delta} \sum_h' \frac{S(\vec{G})}{G^2} \exp(-G^2/4\eta) - 2\, q_p' \left(\frac{\eta}{\pi}\right)^{1/2} \tag{1.6}$$

$$S(\vec{G}) = \sum_p q_p \exp(-i\vec{G}\cdot\vec{r}_p) .$$

The second component ϕ_B is the potential of a lattice of point charges with a superimposed lattice of normalized

Gaussian distributions carrying the opposite charge and is given by

$$\phi_B(i) = \sum_{\ell}' \sum_p \frac{q_p}{|\vec{r}_p|} F(\eta^{1/2} |\vec{r}-\vec{r}_p|) \qquad (1.7)$$

$$F(x) = 2\pi^{-1/2} \int_x^{\infty} e^{-t^2} dt; \quad x = \eta^{1/2}|\vec{r}-\vec{r}_p| .$$

The symbols have the following meaning:

q_p': the charge of the i^{th} ion with position vector $\vec{r}_p' = 0$;

$\vec{r} = l_1\vec{a} + l_2\vec{b} + l_3\vec{c}$, a lattice translation vector in real space with integers l_1, l_2, l_3 and fundamental vectors $\vec{a}, \vec{b}, \vec{c}$;

$\vec{r}_p = x_1\vec{a} + x_2\vec{b} + x_3\vec{c}$, a position vector of ions in a nonprimitive unit cell with fractional coordinates x_1, x_2, x_3, and q_p, the associated charge;

$\vec{G} = 2\,(h_1\vec{a}^* + h_2\vec{b}^* + h_3\vec{c}^*)$, a reciprocal lattice vector with integers h_1, h_2, h_3, and fundamental vectors $\vec{a}^*$, $\vec{b}^*$, $\vec{c}^*$.

$\sum_h'$, the summation over all h_1, h_2, h_3 except $h_1 = h_2 = h_3 = 0$;

$\sum_p$, the summation over all positions p (including p');

$\sum_{\ell}'$, the summation over all l_1, l_2, l_3 except $l_1 = l_2 = l_3 = 0$ when $p = p'$;

Δ, the unit cell volume;

η, the Gaussian half-width, an adjustable parameter.

The total potential ($\phi_i = \phi_A + \phi_B$), which is the potential of a lattice of point charges, will converge with proper choice of η (16) but will be independent of η since the Gaussian terms will cancel in the sum.

The expression for the Madelung energy, in appropriate units, is

$$U \text{ (kcal/mole)} = 332 \sum_i q_i \phi_i / 2 K \qquad (1.8)$$

where ϕ_i is in units of Å^{-1}, q_i is the charge in coulombs at the i^{th} site, K is the total number of formula units per unit cell, and the summation is over all sites in the unit cell.

A FORTRAN program PALS (Potential At a Lattice Site) was written to calculate site potentials and Madelung energies for any crystal system and is given in the Appendix.

Madelung energies for stoichiometric ionic solids are calculated in a straightforward manner. In a non-stoichiometric crystal, an average Madelung energy is calculated, where the vacancies are restricted to, but randomly distributed over, sites on a particular sublattice. In a mean field approximation, this situation is equated with distributing fractional ion charges equally over all

sublattice sites. This is formally represented as a fractional site occupancy f = m/N (m and N are the number of filled and the total number of sublattice sites, respectively). The charge q_i in the Ewald expression becomes $f \cdot z_i$ for the fractionally occupied ion sites, where z_i is the ionic charge of ion i. The anion and cation in $Sc_{0.8}S$ were assigned the charges -2 and +2.48 (for neutral $M_{0.8}X$), respectively.

Configurational Entropy

Consider a lattice of N lattice sites which are occupied by n atoms and N-n vacancies. The number of ways to distribute the atoms and vacancies over N sites is

$$\Omega = N!/(N-n)!n! \quad . \tag{1.9}$$

The entropy associated with Ω configurations of atoms is

$$S_{con} = - k \ln \Omega \quad , \tag{1.10}$$

where k is the Boltzmann constant. Applying the Stirling approximation ($\ln n! = n \ln n - n$) and defining χ_o and χ_v as the fraction of occupied and vacant sites, respectively, the entropy expression becomes

$$S_{con} = - k N (\chi_o \ln \chi_o + \chi_v \ln \chi_v) \quad . \tag{1.11}$$

The process of vacancy ordering involves distributing a fixed number of vacancies (determined by the crystal stoichiometry) over lattice sites on a given sublattice. One of the restrictions of the proposed model for $Sc_{0.8}S$ is that for a superstructure unit cell containing L metal sites and L nonmetal sites, the vacancies are concentrated on 1/L of the metal sites. The metal-to-nonmetal ratio ρ is

$$\rho = [(L-1) + \chi_o]/L \tag{1.12}$$

Solving for χ_o and χ_v $(= 1 - \chi_o)$ and substituting into Eqn. 1.11, the entropy expression per mole $Sc_{0.8}S$ is

$$S_{con} = -\frac{R}{L}\{[L(\rho-1) + 1]\ \ln[L(\rho-1) + 1] + L(\rho-1)\ \ln\ L(\rho-1)\} \tag{1.13}$$

Short-Range Order

The mean field approximation, as described above, treated the occupancy of the metal sublattice as a probability distribution where each site had an equal probability of being occupied, and the probability was determined by the stoichiometry. The first-order correction to this approximation would be to consider the occupancy of one site correlated to the status of other sites. For the case of random particle distribution, the particle distribution function $f_i^{(1)}$ is equal to the probability that a

particular site is occupied without regard to any other sites; $f_{ij}^{(2)}$ is the probability that two particular sites i and j will be occupied without regard to other sites, similarly for $f_{ijk}^{(3)}$, etc.

The short-range correction to the crystal energy considering pairwise correlation only is

$$U_{SR} = \frac{1}{2} \sum_{i \neq j} \sum_{j} \{f_{ij}^{(2)} - [f_i^{(1)}]^2\} \frac{q_i q_j}{|\vec{r}_{ij}|} . \qquad (1.14)$$

In accord with the theory of the grand canonical ensemble (17), one considers an ensemble of lattices each having a variable number of occupied sites. The probability that a randomly selected ensemble will contain particles with one particle at site x_1, a second at x_2, etc., at time t, is denoted $F^{(n)}$. The configurational entropy for a finite lattice of N total sites, in terms of the distribution function $F^{(n)}$, may be expressed as

$$S_{con} = - k \sum_{n=o}^{N} \frac{1}{n!} \langle F^{(n)} \ln F^{(n)} \rangle_{a_1}^{a_n} . \qquad (1.15)$$

The distribution function $f^{(n)}$ described previously, the probability that n specified sites are filled without regard to the condition of the rest of the lattice, can be expressed in terms of $F^{(n)}$ as (18)

$$f^{(n)} = F^{(n)} + \langle F^{(n+1)} \rangle_{n+1}^{n+1} + \frac{1}{2} \langle F^{(n+2)} \rangle_{n+1}^{n+2} + \cdots$$

$$= \sum_{m=o} \frac{1}{m!} \langle F^{(n+m)} \rangle_{n+1}^{n+m} \qquad (1.16)$$

where, by definition

$$\langle F \rangle_{n+1}^{n+m} = \sum_{x_{n+1}} \sum_{x_{n+2}} \cdots \sum_{x_{n+m}} F$$

for $m \geq 1$, and $\langle F \rangle_{n+1}^{n} = F$. The symbol $\sum_{x_{n+i}}$ denotes a sum over all lattice sites of the particle n+i. The first term in Eqn. 1.15 represents the probability of observing n particles at specified sites with no other particles on the lattice; the second term represents the probability of observing n particles with one other particle on the lattice, etc. The factor 1/m! occurs in the m^{th} term since each of the m sums is carried out over the entire lattice, resulting in one configuration occurring m! times. An inverse relationship (18) also exists

$$F^{(n)} = \sum_{m=o} \frac{(-1)^m}{m!} \langle f^{(n+m)} \rangle_{n+1}^{n+m} . \qquad (1.17)$$

This can be verified by the substitution of Eqn. 1.17 into Eqn. 1.16.

Making the approximation that out of n+m total particles only n are correlated and the remaining m particles are

distributed according to the single particle distribution function

$$f^{(n+m)} = f^{(n)}[f^{(1)}]^m, \tag{1.18}$$

Eqn. 1.17 then becomes

$$F^{(n)} = f^{(n)}[1 - f^{(n)}]^{N-n}, \tag{1.19}$$

where N is the total number of sites available on the lattice. Substitution of Eqn. 1.19 into Eqn. 1.15, and extracting only the contribution of pairwise correlation, the total configurational entropy is (19)

$$S_{con} = - kN[\chi_o \ln \chi_o + \chi_v \ln \chi_v] - \frac{k}{2} \sum_{i \neq j} \sum_{j} f_{ij}^{(2)} \ln \frac{f_{ij}^{(2)}}{[f^{(1)}]^2} \tag{1.20}$$

The first term in Eqn. 1.20 is the configurational entropy of a lattice of uncorrelated particles (see Eqn. 1.11); therefore, the correction for pairwise correlation is the second term.

Application of the Model

A group of superstructures of the NaCl structure type which could result from vacancy ordering was generated in the following way. The group was limited to primitive superstructure cells containing five $Sc_{0.8}S$ units or less. Ordered triples of noncoplanar vectors were systematically

chosen from among the translational symmetry operation of an fcc array, the sublattice of metal atoms in a NaCl structure. This triplet of vectors defined the sublattice of fractional occupancy by metal atoms and a new superstructure cell.

An arbitrary cell so constructed is not necessarily a unique description of the lattice, however. Niggli (20) has defined the reduced cell as a primitive cell constructed of the three shortest noncoplanar lattice translations, and has shown a method for identification of the crystal system and Bravais lattice type from a scalar representation of the reduced cell (i.e., $\vec{a}\cdot\vec{a}$, $\vec{b}\cdot\vec{b}$, $\vec{a}\cdot\vec{b}$, $\vec{b}\cdot\vec{c}$, etc., where $\vec{a}$, $\vec{b}$, $\vec{c}$ are the shortest translation vectors). The reduced cell vectors may be obtained from any arbitrary set of primitive vectors by a procedure described by Buerger (21) and extended by Santoro and Mighell (22).

A FORTRAN program GEMS (GEnerate Metal Sublattices) was written to generate sublattices of reduced occupancy, compute reduced cell vectors and their scalar representation, and delete symmetrically equivalent orderings. The conventional cell was deduced using Niggli's criteria (20).

A third program CELL was written to transform the atom coordinates in the NaCl lattice into atom coordinates in terms of the superstructure cell. In this way, each new

superstructure could be described as the superposition of three sublattices: a sublattice of nonmetal atoms, a sublattice totally occupied by metal atoms, and a third sublattice fractionally occupied by metal atoms. The unit cells and space groups are listed in columns 2 and 3 of Table 1.2 (page 26).

EXPERIMENTAL

Sample Preparation and Characterization

Scandium monosulfide was prepared by direct combination of stoichiometric amounts of scandium, rolled to 0.2 mm thickness and electropolished (Ames Laboratory) and sulfur (Ventron, 99.999% purity); also, a small amount of I_2 was added as a transport agent. The elements reacted at 700-800°C for several weeks in evacuated and sealed fused silica tubes. The resulting inhomogeneous material was annealed in an inductively heated W Knudsen cell at 1600°C in high vacuum (a residual pressure less than 10^{-6} torr). Nonstoichiometric sulfides with compositions between $Sc_{1.00}S$ and $Sc_{0.81}S$ (the congruent composition) were prepared by increasing the temperature at which and the length of time for which the monosulfide was inductively heated.

The prepared material was composition analyzed by combustion of a weighed portion of $Sc_{1-x}S$, contained in a Pt crucible, to Sc_2O_3 at 900°C in a muffle furnace. A mole ratio Sc/S could be obtained to an accuracy of ±0.005 with a sample size between 50-75 mg.

X-ray powder diffraction patterns, utilizing a Guinier-Hägg forward focussing camera (Cu K_{α_1}, radiation, 1.5406 Å wavelength; Si internal standard, a = 5.43088 Å)

were used to analyze for the crystal phases present and to monitor changes in the lattice constants.

High Temperature X-ray Diffraction

A Guinier-Simon X-ray powder diffraction camera (Cu K_{α_1}, radiation), with temperature controlling and programming capabilities, was used to examine the vacancy ordering in $Sc_{0.81}S$ over the temperature range 100 - 750°C. The finely powdered sample was contained in an evacuated and sealed 0.3 mm quartz capillary.

Weak superstructure lines corresponding to the $R\bar{3}m$ ordering were observed at temperatures below, but not above 700 ± 20°C, indicating that the order-disorder transition occurs at approximately 700°C. There was no indication of a two-phase region separating the phases, suggestive of a second-order transition (23). In addition, the transition from $Fm3m$ to $R\bar{3}m$, with a doubling of the periodicity along the body diagonal, meets all four conditions required of a second-order phase change by the Landau Theory (24). The approximate d-spacings and corresponding h, k, l values for the observed diffraction lines are given in Table 1.1.

Table 1.1. Approximate d-spacings and corresponding h, k, l values for observed diffraction lines

Temperature Range (°C)	d-Spacing	h k l[a] $R\bar{3}m$	h k l $Fm3m$
T > 700	5.97	0 0 3	not allowed
T > 700	3.12	1 0 1	not allowed
100-700	2.58	1 0 4	2 0 0
100-700	1.826	0 1 8; 1 1 0	2 2 0
100-700	1.491	0 2 4; 0 0, 12	2 2 2
100-700	1.290	2 0 8	4 0 0

[a]Hexagonal indices.

RESULTS AND DISCUSSION

The Madelung energy, configurational entropy, and change in the free energy ($\Delta A = \Delta U - T\Delta S$) at the ordering temperature T = 700°C, calculated for each generated superstructure, are reported in columns 5, 6 and 7 of Table 1.2. These results include only long-range ordering effects.

The short-range contribution to the free energy may be constructed from U_{SR} (Eqn. 1.14) and S_{SR} (Eqn. 1.20), assuming the pair correlation probabilities $f_{ij}^{(2)}$ to be functions only of the distance separating the ions. Minimization of the free energy with respect to the set of $f_{ij}^{(2)}$ and subject to the constraint that the average fractional occupancy of the cation sites was that of the experimental sample (0.8), led to the prediction that the probability of occupancy of nearest neighbor cation sites was zero.

This result is inconsistent with the observed long-range ordering symmetry and reflects the consequences of an energy term that overwhelmed the short-range entropy term.

It has been shown that the coulombic model fails seriously in predicting cation vacancy ordering in defect scandium monosulfide in the following ways: 1) the model results in an ordering temperature for the observed transition which is grossly incorrect ($T = \Delta U/\Delta S = 42{,}000$ K!);

Table 1.2. Space groups, lattice parameters, lattice energy, configurational entropy and change in the free energy for the ordered superstructures

Volume[a]	Space Group	Lattice Parameters (Å, deg)	-U (kcal mole^{-1})	S (cal mole^{-1}deg^{-1})	$\Delta A_{973\ K}$ (kcal mole^{-1})
1	Fm3m	a = 5.17	899.0	0.976	0
2	P4/mmm	a = 3.65 c = 5.17	915.8	0.663	-16.5
2	R$\bar{3}$m	a = 3.65 c = 17.89	912.1	0.663	-12.8
3	Immm	a = 10.96 b = 5.17 c = 3.65	931.2	0.451	-31.8
3	I4/mmm	a = 3.65 c = 15.50	917.9	0.451	-18.4
3	P$\bar{3}$m 1	a = 3.65 c = 8.95	904.3	0.451	- 4.8
4	C2/m	a = 12.11 b = 3.65 c = 6.33 β = 100.0	941.2	0.266	-41.5

[a]Volume of generated primitive cell/volume of rock salt primitive cell.

Table 1.2. (Continued)

Volume[a]	Space Group	Lattice Parameters (Å, deg)	-U (kcal mole^{-1})	S (cal mole^{-1}deg^{-1})	ΔA_{973K} (kcal mole^{-1})
4	Pmmm	a = 5.17 b = 7.30 c = 3.65	937.7	0.266	-38.1
4	Cmmm	a = 7.30 b = 10.33 c = 3.65	941.6	0.266	-42.0
4	P4/mmm	a = 3.65 c = 10.33	904.3	0.266	- 4.6
4	I4/mmm	a = 5.17 c = 10.33	949.9	0.266	-50.3
4	R$\bar{3}$m	a = 3.65 c = 35.78	875.9	0.266	23.7
4	Pm3m	a = 5.17	949.0	0.266	-49.4
5	C2/m	a = 12.11 b = 3.65 c = 8.95 β = 119.5	946.2	0.057	-46.4
5	Immm	a = 5.17 b = 18.26 c = 3.65	936.3	0.057	-36.5

Table 1.2. (Continued)

Volume[a]	Space Group	Lattice Parameters (Å, deg)	-U (kcal $mole^{-1}$)	S (cal $mole^{-1}deg^{-1}$)	$\Delta A_{973\ K}$ (kcal $mole^{-1}$)
5	I4/m	a = 8.17 c = 5.17	962.6	0.057	-62.8
5	I4/mmm	a = 3.65 b = 25.83	875.4	0.057	24.4
5	$R\bar{3}m$	a = 3.65 b = 44.73	827.5	0.057	-72.3

2) the model predicts that a number of long range ordered structures would be more stable than the observed ordered structure and by as much as 60 kcal, not just a few kcal; 3) the model predicts an overwhelming short-range ordering that is not observed. In addition, it has been observed that the partial molar enthalpy of Sc in the defect solid is overestimated by 115 kcal using the ionic model (25).

These conclusions are based upon the most simplistic coulombic model, i.e., neglecting repulsive and polarization corrections and a variety of possible short-range effects. However, the comparison of the stabilities of the various possible long-range ordered structures would continue to predict that defect orderings other than the observed $R\bar{3}m$ ordering for $Sc_{0.8}S$ would be stable, even if these correction terms and short-range effects were included. Thus, it can be safely concluded that the observed long-range ordering does not result from coulombic interactions.

REFERENCES

1. Watanabe, D.; Castles, J. R.; Jostons, A.; Malin, A. S. Acta Cryst. 1967, 23, 307.

2. Bowman, A. L.; Wallace, T. C.; Yarnell, J. L.; Wenzel, G. R. Acta Cryst. 1966, 21, 843.

3. Dismukes, J. P.; White, J. G. Inorg. Chem. 1964, 3, 1220.

4. Conard, B. R.; Franzen, H. F. In "Chemistry of Extended Defects in Non-Metallic Solids"; Eyring, L.; O'Keefe, M., Eds.; North-Holland: Amsterdam, 1970; p. 207.

5. Hariharan, A. V.; Franzen, H. F. 1978 Summer Symposium on Solid State Chemistry, Laramie, Wyoming, Aug. 1978.

6. Bertaut, E. F. Acta Cryst. 1953, 6, 557.

7. O'Keefe, M.; Valigi, M. J. Chem. Phys. 1969, 50, 1490.

8. Waddington, T. C. In "Advances in Inorganic Chemistry and Radiochemistry"; Emeléus, H. J.; Sharpe, A. G., Eds.; Academic Press: New York, 1959; Vol. 1, p. 158.

9. Tosi, M. P. Solid State Phys. 1964, 16, 1.

10. Madelung, E. Physik. Z. 1918, 19, 524.

11. Quane, D. J. Chem. Ed. 1970, 47, 396.

12. Burrows, E. L.; Kettle, S. F. A. J. Chem. Ed. 1975, 52, 58.

13. Evjen, H. M. Phys. Rev. 1932, 39, 675.

14. Ewald, P. P. Ann. Physik 1921, 64, 253.

15. Kittel, C. "Introduction to Solid State Physics", 2nd ed.; Wiley: New York, 1963; p. 571.

16. Van Gool, W.; Piken, A. G. J. Mater. Sci. 1969, 4, 95.

17. Davidson, N. "Statistical Mechanics"; McGraw-Hill: New York, 1962; Chapter 13.

18. Hoffman, D. K. J. Chem. Phys. 1976, 65, 95.

19. Merrick, J.; Hoffman, D. K., Iowa State University, Ames, IA, unpublished results.

20. Niggli, P. In "Handbuch der Experimentalphysik"; Akademische Verlagsgesellschaft: Leipzig, 1928; Vol. 7, Part 1.

21. Buerger, M. J. Z. Kristallogr. 1957, 109, 42.

22. Santoro, A.; Mighell, A. D. Acta Cryst. 1970, A26, 124.

23. Franzen, H. F.; Gerstein, B. C. A. I. Ch. E. J. 1966, 12, 364.

24. Landau, L. D.; Lifshitz, E. M. "Statistical Physics"; Pergamon: London, 1962; Chapter 14.

25. Tuenge, R. T.; Laabs, F.; Franzen, H. F. J. Chem. Phys. 1976, 65, 2400.

SECTION II. THERMODYNAMICS OF ScP

INTRODUCTION

Dismukes and White (1) have proposed a formula for defect scandium monosulfide $Sc^{3+}(e^-)S^{2-}$, in which (e^-) represents a delocalized electron participating in metal-metal bonding. A similar formula for scandium monophosphide, which is isostructural with the monosulfide and which has one less electron, would be $Sc^{3+}P^{3-}$; where there is no longer a metal-metal bonding (delocalized electron) contribution. A comparison of properties (structural, electronic, and thermodynamic) between the sulfide and phosphide would aid in the understanding of these metal-metal bonding interactions.

ScP crystallizes in the NaCl-type crystal structure (a = 5.312 Å (2); 5.302 ± 0.05 kχ (3); 5.3088 ± 0.0005 Å (4)), has a melting point greater than 2000°C (3), and is a semiconductor with a 1.1 eV band gap (4). By a comparison of the properties, ScP and ScS are found to be very similar materials. (See Table 1 for properties of ScS). Thermodynamic data for ScS have been reported (5); however, no complementary data are known for ScP, nor for transition metal phosphides in general (6).

It was the purpose of this study to carry out a high temperature vaporization study of the scandium phosphide system, utilizing mass spectrometry and the target

collection Knudsen effusion technique, and by comparison to a similar study on ScS gain insight into the stabilizing or destabilizing effects of metal-metal bonding.

THEORY AND METHOD

Mass Spectrometric Measurement

Mass spectrometry has been used extensively in the investigation of the vapor-condensed phase equilibrium of various systems. These studies have led to the identification of the gaseous species, and to the determination of thermodynamic properties for the gaseous species and the condensed phases from which they originate (7,8). A quadrupole mass spectrometer, as used in this investigation, consists of a vapor source, which provides a molecular beam arising from the vaporization of the condensed material; an ion source which ionizes the neutral molecular or atomic species and directs the ion beam onto the analyzer; a quadrupole analyzer consisting of four rods on which rf and dc potentials in varying ratios are superimposed, therefore allowing for mass separation; and an ion current detector. In this study, the mass spectrometer was employed to identify the vapor species in equilibrium with solid ScP at high temperatures, and to measure appearance potentials of each vapor species to enable identification of the parent ions.

Knudsen Effusion Vapor Pressure Measurements

The Gibbs phase rule

$$F = C - P + 2 \tag{2.1}$$

defines the conditions by which the measurement of partial pressures will lead to meaningful equilibrium data. Consider a binary system in which the solid and vapor are in equilibrium. The number of components C is 2, the number of phases in equilibrium P is 2, therefore, the number of independent intensive variables F is also 2. If congruent vaporization occurs such that the vapor and solid have the same composition, the system is univarient, i.e., at a fixed temperature the pressure will also be fixed. Various methods for vapor pressure measurement are described in a review by Cater (9). The target collection Knudsen effusion technique was employed in this study.

Knudsen (10) derived the relationship for the rate at which molecules of the i^{th} gaseous species effuse through a small, knife-edged orifice of area A, as a function of partial pressure P_i, mass m_i, and temperature T

$$\frac{d}{dt}\,(N_i/A) = P_i/(2\pi\, m_i\, kT)^{1/2}, \tag{2.2}$$

where N_i is the number of effusing molecules and k is Boltzmann's constant. Clausing (11) proposed a correction

factor K_c for nonideal orifices which accounts for molecules which strike the orifice walls and re-enter the cell, rather than effusing through the orifice. In the case of a target collection experiment, the fraction of the effusate striking a circular target of radius R, placed a distance L coaxially with the orifice, is $F = R^2/(R^2 + L^2)$. The Knudsen equation for the target collection set up corrected for a nonideal orifice, and in terms of the weight loss W_i (grams), the orifice area A (cm^2), the time t(sec), the partial pressure P_i (atm) of the ith species, the temperature T(K), and M_i the molecular weight becomes

$$P_i \text{ (atm)} = 0.02256\ W_i T^{1/2}/A\ K_c\ Ft\ M_i^{1/2} \qquad (2.3)$$

Calculation of Thermodynamic Quantities

For systems in which the vapor pressure is less than one atmosphere, the vapor species may be treated as a mixture of ideal gases and an equilibrium constant K may be calculated for a particular reaction, from the partial pressures P_i. The standard free energy change at temperature T is

$$\Delta G_T^\circ = -RT \ln K. \qquad (2.4)$$

Combining Eqn. 2.4 with the basic equation

$$\Delta G_T^\circ = \Delta H_T^\circ - T\ \Delta S_T^\circ \qquad (2.5)$$

the following equation results:

$$2.303\ R\ \log\ K = -\Delta H^{\circ}_{T}/T + \Delta S^{\circ}_{T}. \qquad (2.6)$$

Assuming the heat capacities of the reactants and products are constant in the temperature interval of experimental measurement, a plot of 2.303 R log K versus 1/T is linear with slope $-\Delta H^{\circ}_{T}$ and intercept ΔS°_{T}. The data points are fitted to the best straight line by a least squares technique and the resulting enthalpy and entropy are assigned to a median temperature $T_{med} = 2/(1/T_{lower} + 1/T_{upper})$. This treatment is referred to as the second-law method. The second-law enthalpy and entropy at T_{med} may be reduced to the enthalpy and entropy at a reference temperature by the appropriate heat capacity function

$$H_T - H_{298} = \int_{298}^{T} C_p(T)\ dT \qquad (2.7)$$

$$S_T - S_{298} = \int_{298}^{T} C_p(T)/T\ dT. \qquad (2.8)$$

The heat capacities of inorganic compounds may be estimated empirically (12).

An alternate treatment, the third-law method, is to calculate ΔH°_{298} from each experimental point by computing the change in the free energy function (fef) for a reaction according to

$$\Delta fef_T = (\Delta G_T - H^{\circ}_{298})/T. \qquad (2.9)$$

Combining Eqn. 2.9 with Eqn. 2.4, the following equation is obtained:

$$\Delta H^{\circ}_{298} = -T(R \ln K_T + \Delta fef_T). \qquad (2.10)$$

The third-law enthalpy change is the average ΔH°_{298} calculated from each data point. The estimation of C_p and S°_{298} is necessary for species where fef has not been measured.

EXPERIMENTAL

Sample Preparation and Characterization

Scandium monophosphide was prepared in the same manner as previously described for scandium monosulfide in Section I. The resulting annealed material had a gray metallic luster and was easily powdered. X-ray powder diffraction patterns of the homogeneous material showed the rock salt structure of ScP, with a lattice parameter of 5.302 ± 0.001 Å.

A preliminary vaporization of ScP was conducted by repeatedly heating a previously annealed sample of ScP in high vacuum to temperature in the range 1950 to 2373 K for several hours and following the X-ray diffraction patterns of the residue after each heating. In all cases, the powder patterns showed that only the fcc ScP phase was present and that the lattice constant remained identical to that of the starting material throughout the heating procedure. It was also observed that the sample did not melt at temperatures as high as 2373 K.

Mass Spectrometric Experiment

An EAI quadrupole mass spectrometer (Model 2508 - axial beam with paraxial electron multiplier) was used to study the vapor species effusing from a tungsten Knudsen cell

containing ScP. The equipment and operating procedures have been previously described (13).

A Leeds and Northrup disappearing filament optical pyrometer which was sighted into a black-body hole in the base of the Knudsen cell was used for temperature measurements. Ion intensities were taken as the difference between peak heights obtained by scanning the mass range of interest with the shutter open and the backgrounds in the same region with the shutter closed. Measurements were made in the medium mass range of the spectrometer (10 - 150 amu) using an electron energy of 45 eV at 2 mA emission current. A well-annealed and homogenized sample of ScP was used. Peak intensities at 31, 45 and 62 amu were measured simultaneously over the temperature range 1767 to 2105 K.

Data for shutter profiles of the effusing vapor species appearing at 31, 45, and 62 amu, and an appearance potential curve for the 45 amu species were obtained with the sample at 1990 K. The linearly extrapolated appearance potential for the 45 amu species was 6.5 ± 0.4 eV (1st Ionization Potential, Sc 6.54 eV (14)), using CO_2 (1st Ionization Potential, 13.8 ± 0.3 eV (15)) as a calibrant to the energy scale.

Knudsen Effusion Study

A target collection procedure (13) was used to measure absolute rates of effusion of the vapor in equilibrium with ScP over the temperature range 1950-2209 K (IPTS-68 (16)). A schematic of the vacuum line apparatus used in shown in Fig. 2.1. A well-anealed and homogenized sample of ScP (150 mg) was placed in a high density tungsten crucible insert, which in turn was contained in a symmetric tungsten effusion cell. A cell with orifice diameter 1.773 ± 0.020 mm (at 2049 K) was used over the temperature range 1950-2148 K for two experiments (8 points and 18 points, respectively), and a cell with orifice diameter 0.922 ± 0.010 mm (at 2164 K) was used over the temperature range 2121-2209 K (8 points).

Vapor deposits were collected on liquid nitrogen-cooled, high purity aluminum targets. Exposure times, defined by the opening or closing of a shutter located between the effusion cell and target, were monitored with a precision laboratory timer. Targets were collected both on raising and lowering the temperature to assure thermodynamic equilibrium in the system.

X-ray Fluorescence Analysis of the Targets

The effusates that collected on the targets were analyzed for scandium by the X-ray fluorescence technique.

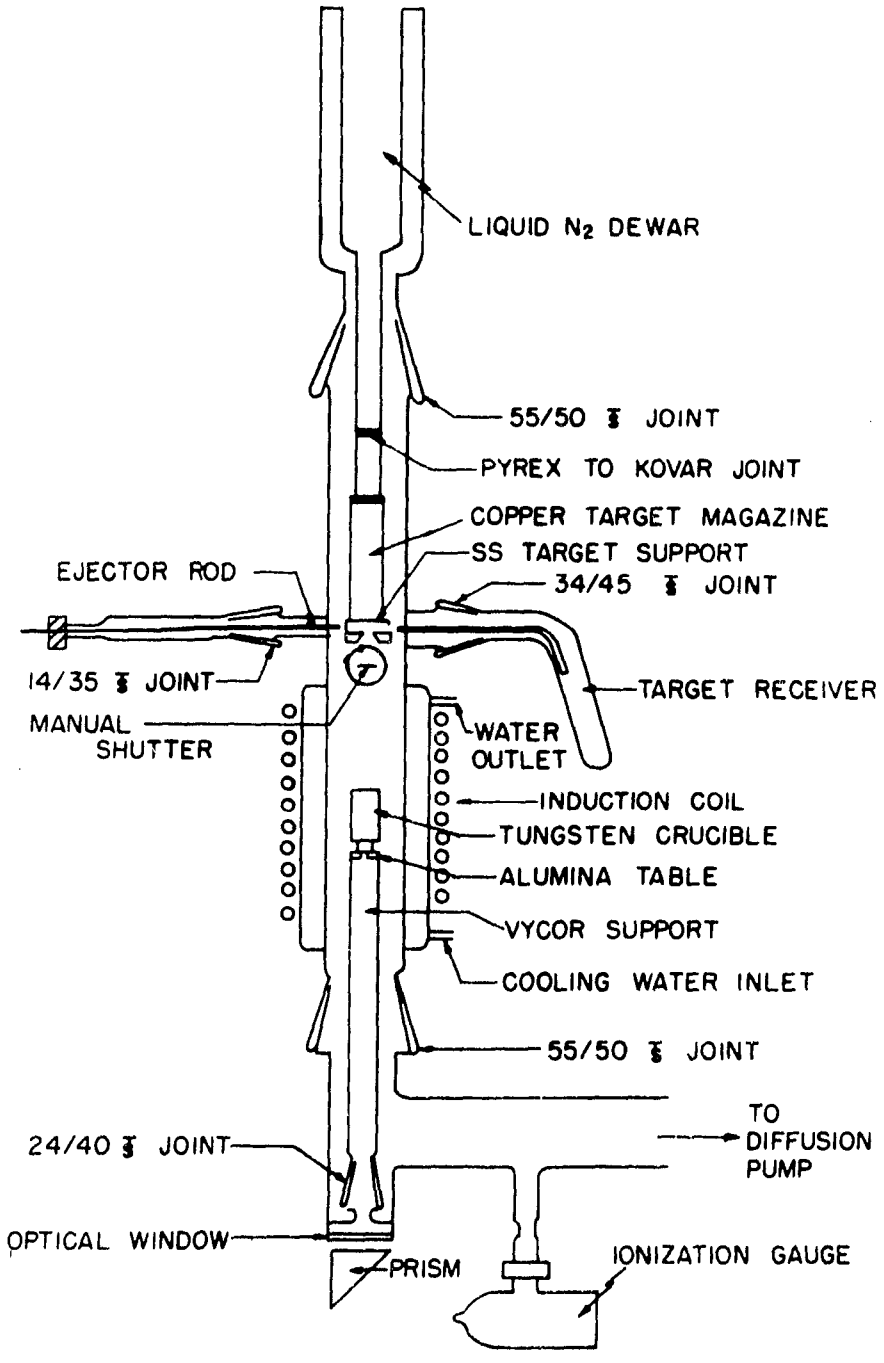

Fig. 2.1. Schematic diagram of vacuum line apparatus used for target collection experiments on scandium phosphide

The procedure used to calibrate for microgram quantities of scandium was as follows: Ten calibration targets were prepared by pipetting 50 µl of ten individual Sc stock solutions containing 1-10 µl Sc, respectively. These solutions were delivered dropwise onto a 2 cm^2 area of the target and evaporated under an infra-red lamp. The calibration targets were counted by X-ray fluorescence in a Tracer Northern Energy Dispersive spectrometer by F. Laabs of the Ames Laboratory, Spectrochemical Services Group. The exciting radiation used was Mo (15 kV, 0.11 mA); the Sc Kα peak (4.120 kV) was counted for 1500 seconds. A blank target was also counted to allow for background subtraction. A calibration curve relating net counts to micrograms (µg) Sc was obtained by a linear least squares treatment. The overall standard deviation in the measurement of µg Sc was ±0.28. Targets containing 4.9 and 5.9 µg Sc, respectively, were selected as standards and were counted with each set of experimental targets. This allowed normalization of the net counts from each experimental set to the net counts obtained during calibration. Normalization factors ranged from 0.99 to 1.01.

RESULTS

From the high temperature annealing and vaporization of ScP, followed by X-ray powder diffraction analysis of the residues, the congruent vaporization of the compound was established. There was no indication of any stoichiometry changes in scandium monophosphide.

The shutterable ion intensities, observed at 31, 45 and 62 amu during the mass spectrometric experiment, were identified as resulting from the ionized species P^+, Sc^+ and P_2^+, respectively. No gaseous molecular ions corresponding to ScO^+ or ScP^+ were observed over the experimental temperature range. The shutter profiles were indicative of the Sc species effusing strictly from the orifice and the phosphorus species effusing principally from the orifice but with observable effects arising from species vaporizing from the region within the radiation shields. The appearance potential measurement indicated Sc as a primary gaseous species and not a dissociative product from the molecular ScP. Thus, the following net reactions for the vaporization of ScP may be written

$$ScP(s) = Sc(g) + 1/2\ P_2(g) \qquad (2.11)$$

$$ScP(s) = Sc(g) + P(g). \qquad (2.12)$$

Scandium partial pressures were calculated according to the Knudsen effusion equation (Eqn. 2.2) for each of the

36 data points from three independent target collection experiments. The Clausing correction factor K_c was taken as unity for the near-ideal orifices (17). The experimental data and calculated pressures are given in Table 2.1. An unweighted linear least squares treatment of log P_{Sc} versus 1/T resulted in the equation

$$\log P_{Sc}\,(\text{atm}) = -(28159 \pm 321)/T + (8.10 \pm 0.15). \quad (2.13)$$

Conditions of material balance and congruent vaporization, combined with the Knudsen effusion, lead to the relation (Eqn. 2.14) between individual phosphorus partial pressures (P_P, P_{P_2}) and the measured scandium partial pressure (P_{Sc})

$$P_{Sc}/M_{Sc}{}^{1/2} = P_{P}/M_{P}{}^{1/2} + 2P_{P_2}/M_{P_2}{}^{1/2} . \quad (2.14)$$

The equilibrium constant $K_P(=P_P{}^2/P_{P_2})$ for the dissociation reaction may be calculated from the Gibbs free energy function for P(g) (18), and P_2(g) (18), and ΔH°_{298} of dissociation (116.90 ± 0.10 kcal mole^{-1} (19)). A linear fit (log K_P = -26036/T + 6.246) was used to calculate K_P, and in turn, the equilibrium partial pressures P_{P_2} and P_P at each experimental temperature. P_{P_2} and P_P were of the same order of magnitude with P_{P_2} being slightly greater. Linear least squares treatment of individual partial pressures gave

Table 2.1. Target collection Knudsen effusion data

	Temperature (K)	Time (min)	Sc Collected (μg)	$P_{Sc} \times 10^6$ [a,b] (atm)	ΔH°_{298} [c] (kcal mole^{-1})
1.	1972	145	4.75	0.63	252.9
2.	2055	46	5.56	2.35	252.7
3.	2056	45	5.68	2.47	252.5
4.	2034	60	5.92	1.91	252.0
5.	2005	90	5.17	1.11	252.6
6.	2078	35	6.69	3.76	251.8
7.	2104	25	6.15	4.83	252.7
8.	2104	25	6.78	5.37	252.0
9.	1950	240	5.97	0.47	252.4
10.	1986	122	5.60	0.88	252.1
11.	1986	120	4.90	0.78	252.9
12.	1970	151	4.87	0.62	252.8
13.	2021	71	5.12	1.40	252.7
14.	2020	70	5.23	1.44	252.4
15.	2004	92	5.69	1.19	252.1
16.	2049	49	5.98	2.38	252.0
17.	2065	35	5.60	3.10	251.9
18.	2086	27	5.80	4.22	251.8
19.	2086	26	5.36	4.13	252.0

[a] Orifice Area: (#1-26) $2.469 \cdot 10^{-2}$ cm^2 at 2049 K
(#27-34) $6.669 \cdot 10^{-3}$ cm^2 at 2164 K

[b] Collection Factors: (#1-8) 0.00527
(#9-26) 0.00528
(#27-34) 0.00525

[c] ΔH°_{298} from Reaction 2.12: ScP(s) = Sc(g) + P(g).

Table 2.1. (Continued)

	Temperature (K)	Time (min)	Sc Collected (μg)	$P_{Sc} \times 10^6$ [a,b] (atm)	ΔH°_{298} [c] (kcal mole^{-1})
20.	2064	37	5.49	2.90	252.2
21.	2098	26	6.62	5.01	251.8
22.	2121	17	6.06	7.06	251.7
23.	2148	13	6.32	9.61	252.1
24.	2147	13	6.65	10.42	251.5
25.	2127	15	5.67	7.49	251.9
26.	2106	23	6.21	5.26	252.3
27.	2121	51	4.30	6.24	252.5
28.	2150	35	4.40	9.50	252.4
29.	2168	28	4.58	12.42	252.2
30.	2186	22	4.75	16.21	252.0
31.	2209	12	3.71	23.97	251.4
32.	2209	12	3.54	22.80	251.8
33.	2196	15	3.61	18.34	252.1
34.	2169	18	3.28	13.64	251.7
				Average	252.2 ± 0.4

$$\log P_{P_2}(\text{atm}) = -(28533 \pm 393)/T + (7.898 \pm 0.189) \quad (2.15)$$

$$\log P_P(\text{atm}) = -(27235 \pm 321)/T + (7.050 \pm 0.154), \quad (2.16)$$

where the uncertainties are standard deviations. The experimental points for P_{Sc} and the calculated least squares lines for P_{P_2} and P_P as a function of temperature are shown in Fig. 2.2.

Equilibrium constants for the congruent vaporizations of Reactions 2.11 and 2.12 may be represented by

$$\log K_1 = -(42426 \pm 376)/T + (12.05 \pm 0.18) \quad (2.17)$$

$$\log K_2 = -(55394 \pm 454)/T + (15.15 \pm 0.22). \quad (2.18)$$

The entropy and enthalpy changes for vaporization at the median temperature (2071 K) are: Reaction 2.11, ΔH°_{298} = 194.1 ± 1.7 kcal mole^{-1}; ΔS°_{2071} = 55.15 ± 0.83 eu; Reaction 2.12, ΔH°_{2071} = 253.5 ± 2.1 kcal mole^{-1}; ΔS°_{2071} = 69.33 ± 1.00 eu.

To reduce the median temperature data to 298 K, the heat capacity of ScP(s) was estimated both at 298 K and at the melting point (2400 K). Addition of heat capacities of the component elements gave $C^\circ_{P,298}$[ScP(s)] = 11.17 eu, and Kubaschewski's approximation (12) yielded $C^\circ_{P,2400}$[ScP(s)] = 14.50 eu. The heat capacity function

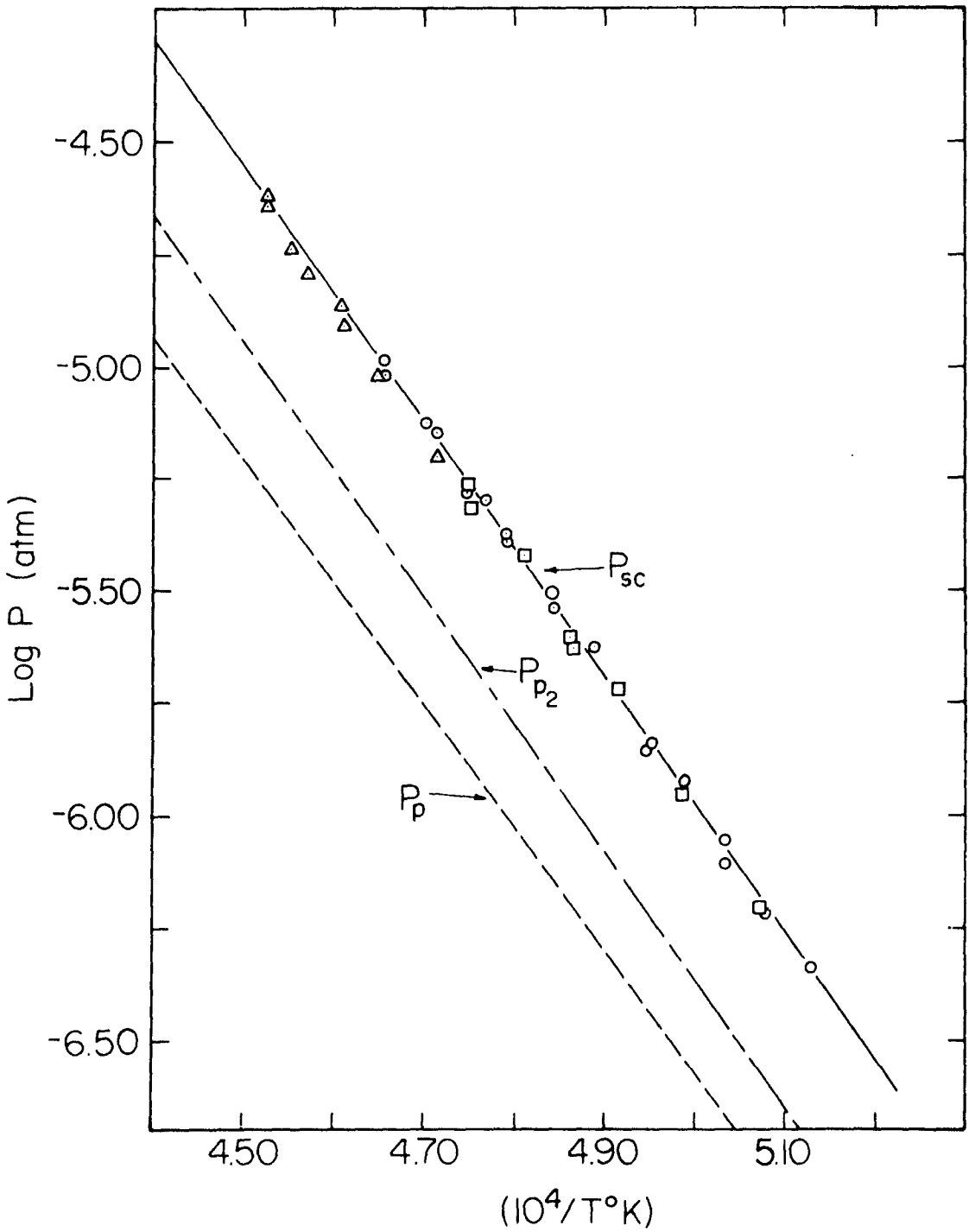

Fig. 2.2. Target collection Knudsen effusion data for ScP. Experimental log P_{Sc}(atm) and calculated log P_P(atm) and log P_{P_2} (atm) vs. $10^4/T$ (1950-2209 K). (□: data points 1-8; o: data points 9-26; △: data points 27-34)

for ScP(s) over the temperature range 298 - 2400 K, with the assumption of a linear variation, may then be represented by

$$C_P^\circ\ [ScP(s)] = 1.58 \times 10^{-4}\ T + 10.70 \qquad (2.19)$$

The enthalpy and entropy functions used to reduce ΔH_T and ΔS_T to 298 K are given in Table 2.2. The errors associated with the enthalpy and entropy functions as a result of the estimates involved in obtaining Eqn. 2.19 were assumed to be ± 1 kcal mole^{-1} and ± 1 eu, respectively.

Results of the second law data treatment including uncertainties associated with data reduction are: Reaction 2.11, ΔH°_{298} = 199.7 ± 2.0 kcal mole^{-1}; ΔS°_{298} = 60.6 ± 1.3 eu; Reaction 2.12, ΔH°_{298} = 258.0 ± 2.3 kcal mole^{-1}; ΔS°_{298} = 73.4 ± 1.4 eu.

Combining these data with entropies and enthalpies of formation for Sc(g) (19) and P(g) (18) (Table 2.2), the enthalpy of formation and the standard entropy of ScP were calculated as: $\Delta H^\circ_{f,298}[ScP(s)]$ = -87.9 ± 2.5 kcal mole^{-1}; $S^\circ_{298}[ScP(s)]$ = 7.3 ± 1.4 eu. The results of the second law treatment are summarized in Table 2.3.

The third law enthalpies for Reaction 2.12 were calculated from the experimentally measured P_{Sc}, the derived P_P, and the Gibbs free energy functions for Sc(g) (19), P(g) (18), and ScP(s) (estimated from the heat capacity

Table 2.2. Thermal functions

		Sc(g)[a]	1/2 P_2(g)[b]	P(g)[b]	ScP(s)[c]
$H^\circ_{2071} - H^\circ_{298}$	(kcal mole^{-1})	8.929	7.746	8.839	22.29 ± 1.0
$S^\circ_{2071} - S^\circ_{298}$	(eu)	9.807	8.290	9.644	23.54 ± 1.0
S°_{298}	(eu)	41.748	26.055 ± 0.05	38.98	10.1 ± 1.0
$\Delta H^\circ_{f,298}$	(kcal mole^{-1})	90.32 ± 1.0	21.34 ± 0.25	79.8 ± 0.05	

[a]Ref. 19.

[b]Ref. 18.

[c]Estimated.

Table 2.3. Thermodynamic results of ScP(s) vaporization

	ΔH°_{2071} (kcal mole^{-1})	ΔS°_{2071} (eu)	ΔH°_{298} (kcal mole^{-1})	ΔS°_{298} (eu)
1. $ScP(s) = Sc(g) + 1/2\ P_2(g)$	194.1 ± 1.7	55.2 ± 0.8	199.7 ± 2.0[a] 193.7 ± 2.8[b]	60.6 ± 1.3
2. $ScP(s) = Sc(g) + P(g)$	253.5 ± 2.1	69.3 ± 1.0	258.0 ± 2.3[a] 252.2 ± 2.8[b]	73.4 ± 1.4
3. $Sc(s) + P(V,red) = ScP(s)$			-87.9 ± 2.5 -82.1 ± 3.0[b]	-3.65 ± 0.56[c]

[a] 2nd law treatment.

[b] 3rd law treatment, preferred.

[c] Estimated by averaging $\Delta S^\circ_{f,298}$ of LaP and SmP (Ref. 20,21).

function). The standard entropy S°_{298}[ScP(s)] was estimated to be 10.1 ± 1.0 eu by assuming the $\Delta S^{\circ}_{f,298}$ of ScP(s) to be the average of $\Delta S^{\circ}_{f,298}$ of LaP(s) (20) and SmP(s) (21). The calculated third law enthalpy change for Reaction 2.12 is ΔH°_{298} = 252.2 ± 2.8 kcal mole^{-1}, where the uncertainty includes the standard deviation of the experimental data and an uncertainty of ΔFEF of ± 1.4 eu. Table 1.1 includes the individual third law enthalpies as calculated at each experimental temperature.

DISCUSSION

Scandium monophosphide has been found to vaporize congruently in the temperature range 1760-2209 K to produce the vapor species Sc(g), P_2(g), and P(g), as identified by mass spectrometry.

The exact composition of the congruently vaporizing monophosphide has not been established because of the difficulties of quantitatively analyzing for scandium in the presence of phosphorus. In phase studies of other monophosphide systems (CeP (22), PrP (23), GdP (24) ThP (25)), a composition change of 15%, because of phosphorus vacancies, resulted in a 0.5% decrease in the lattice parameter; whereas no variation of the lattice parameter was observed for composition changes of 4% or less. Since no measurable change in the lattice parameter of the vaporization residues from the initial scandium monophosphide composition was observed during the course of this investigation, it was concluded that the congruently vaporizing scandium phosphide phase contains no more than ~4% phosphorus vacancies. Also, phosphorus-rich phases in these systems have been shown to be unstable at high temperatures (6). It was therefore concluded that the congruently vaporizing monophosphide is very nearly $ScP_{1.00}$.

The standard enthalpies of atomization calculated by the second and third law methods agree to within 6 kcal $mole^{-1}$ (2nd Law: $\Delta H^{\circ}_{atm,298}$ = 258.0 ± 2.3 kcal $mole^{-1}$; 3rd Law: $\Delta H^{\circ}_{atom,298}$ = 252.2 ± 2.8 kcal $mole^{-1}$). Experimental heat capacities for ScP(s) have not been reported in the literature, thus it was necessary to estimate both the heat capacities and S°_{298} for ScP(s) to calculate the second and third law thermodynamic data. An uncertainty in the average heat capacity of 1 eu would decrease the second law enthalpy value by ∿2 kcal $mole^{-1}$ and would increase the third law value by ∿2 kcal $mole^{-1}$, thus bringing the two values well within the experimental uncertainties. Additional uncertainty in the third law atomization enthalpy arises from the estimate in S°_{298}. The standard deviation of the individual third law enthalpies corresponding to all experimental temperatures is ±0.4 kcal $mole^{-1}$. The small magnitudes of the deviations indicate that there are no temperature dependent errors in the experiment, and that the significant discrepancy between the second and third law enthalpies may be completely accounted for by uncertainties in the heat capacity function and S°_{298} for ScP(s).

Comparing the atomization enthalpies of ScP(s) ($\Delta H^{\circ}_{atom,298}$ = 252.2 ± 2.8 kcal $mole^{-1}$) and ScS(s) (5) ($\Delta H^{\circ}_{atom,298}$ = 240.3 ± 3.0 kcal $mole^{-1}$), it is found that ScP(s) is more stable than ScS(s) by ∿12 kcal $mole^{-1}$.

It is concluded that, to a first approximation, the delocalized electrons of the metal-metal bonding interactions in ScS lead to destabilization compared to the ScP system, which contains only metal-nonmetal bonding interactions. The destabilization effect will be discussed in more detail in connection with the band structure calculations of ScS.

REFERENCES

1. Dismukes, J. P.; White, J. G. Inorg. Chem. 1966, 3, 1220.

2. Parthé, E.; Parthé, E. Acta Cryst. 1963, 16, 71.

3. Komissarova, L. N.; Men'kov, A. A.; Vasil'eva, L. M. Inorg. Mater. 1965, 1, 1361.

4. Yim, W. M.; Stofko, E. J.; Smith, R. T. J. Appl. Phys. 1972, 43, 254.

5. Tuenge, R. T.; Laabs, F.; Franzen, H. F. J. Chem. Phys. 1976, 65, 2400.

6. Mironov, K. E.; Vasil'eva, I. G.; Pritchina, T. G. Rev. Chim. Minér. 1973, 10, 383.

7. Drowart, J.; Goldfinger, P. Angewandte Chemie, International Edition, 1967, 6(7).

8. Grimley, R. T. In "Characterization of High Temperature Vapors"; Margrave, J. L., Ed.; Wiley: New York, 1967; Chapter 8.

9. Cater, E. D. In "Techniques of Metals Research"; Bunshah, R. F., Series Ed.; Rapp, R. A., Ed.; Interscience: New York, 1970; Vol. IV, Part 1, Chapter 2A.

10. Knudsen, M. Ann. Physik 1909, 29, 179.

11. Clausing, P. Ann. Physik 1932, 12, 961.

12. Kubaschewski, O.; Ünal, H. High Temp.-High Press. 1977, 9, 361. Kubaschewski, O; Evans, E. Ll. "Metallurgical Thermochemistry"; Pergamon: New York, 1958; p. 183.

13. Franzen, H. F.; Hariharan, A. V. J. Chem. Phys. in press.

14. Moore, C. E. "Ionization Potentials and Ionization Limits Derived from the Analysis of Optical Spectra", National Bureau of Standards, 1970, NSRDS-NBS 34.

15. Tanaka, Y.; Jursa, A. S.; LeBlanc, F. J. J. Chem. Phys. 1960, 32, 1199.

16. Douglas, T. B. J. Research Natl. Bur. Stand.-A 1969, 73A, 451.

17. Ward, J.W.; Mulford, R. N. R.; Kahn, M. J. Chem. Phys. 1967, 47, 1710. Ward, J. W.; Mulford, R. N. R.; Bivins, R. L. J. Chem. Phys. 1967, 47, 1718.

18. "JANAF Thermochemical Tables", 2nd ed.; Stull, D. R., Ed.; U. S. Government Printing Office: Washington, D. C., 1971; NSRDS-NBS 37.

19. Hultgren, R.; Desai, P. D., Hawkins, D. T.; Gleiser, M.; Kelley, K. K.; Wagman, D. D. "Selected Values of the Thermodynamic Properties of the Elements"; American Society for Metals: Metals Park, OH, 1973.

20. Mironov, K. E.; Paukov, I. E.; Rakhmenkulov, F. S.; Frolova, G. I. Russ. J. Phys. Chem. 1975, 49, 157.

21. Mironov, K. E.; Paukov, I. E.; Rakhmenkulov, F. S.; Frolova, G. I. Russ. J. Phys. Chem. 1976, 50, 1467.

22. Orio, S. J. Less-Common Metals 1974, 38, 119.

23. Franceschi, E.; Olcese, G. L. J. Phys. Chem. Solids 1969, 30, 903.

24. Mironov, K. E.; Vasil'eva, I. G.; Vasil'eva, Ya. V.; Mironov, Yu, I. Russ. J. Inorg. Chem. 1971, 16, 939.

25. Javorsky, C. A.; Benz, R. J. Nucl. Mater. 1967, 23, 192.

SECTION III. BAND STRUCTURE OF ScS

INTRODUCTION

The motivation for the previously described thermodynamic study of ScP was to obtain a first approximation to the effects of metal-metal bonding in ScS. A more rigorous approach to the extent or importance of metal-metal bonding, however, is possible through quantum mechanical band structure calculations.

Recent collaborative efforts between Bruce Harmon of the Physics Department and Thuy-Hoa Nguyen (1) have made available the computer programs necessary to carry out band structure calculations for binary systems with cubic or hexagonal crystal structures by the LAPW (Linearized Augmented Plane Wave) method. Collaboration with these workers made possible the band structure calculations for ScS (NaCl-structure type) discussed below.

THEORY AND METHOD

LAPW Band Structure Calculations

The nonrelativistic, nonself-consistent LAPW method (2) was selected as the method used to calculate the band structure of ScS. The LAPW method is a modified form of the APW (Augmented Plane Wave) method which has been explained in detail in a text by Loucks (3).

The LAPW method is based upon a muffin-tin approximation to the crystal potential, i.e., within spheres centered at the atomic sites the potential is spherically symmetric, and outside the spheres the potential is constant. The crystal potential V is constructed such that it maintains the periodicity of the lattice

$$V(\vec{r} + \vec{l}) = V(\vec{r}) \tag{3.1}$$

$\vec{r}$: a general real space vector

$\vec{l}$: a real space lattice translation vector

and therefore, the solutions to the Schrödinger equation for the periodic potential must satisfy the Bloch condition. The Bloch theorem states that the eigenfunctions $\psi_{\vec{k}}$ for a periodic potential are of the form of a product of a plane wave $\exp(i\vec{k}\cdot\vec{r})$ and a function $u(\vec{r})$ which has the lattice periodicity

$$\psi_{\vec{k}}(\vec{r}) = \exp(i\vec{k}\cdot\vec{r})\ u_{\vec{k}}(\vec{r}) \tag{3.2}$$

where, $\vec{k}$ is a wavevector which labels the eigenstate and $u_{\vec{k}}(\vec{r} + \vec{l}) = u_{\vec{k}}(\vec{r})$ is a periodic function. It follows that

$$\psi_{\vec{k}}(\vec{r} + \vec{l}) = \exp(i\vec{k}\cdot\vec{l})\ \psi_{\vec{k}}(\vec{r}) \ . \tag{3.3}$$

A general wavevector $\vec{k}$ may be expressed as

$$\vec{k} = \vec{k}_n + \vec{K} \tag{3.4}$$

where, $\vec{k}_n$ is a reduced wavevector (within the first Brillouin zone) and $\vec{K}$ is reciprocal lattice vector. Substituting Eqn. 3.4 into Eqn. 3.3 and noting that $\exp(i\vec{K}\cdot\vec{l}) = 1$ results in the expression

$$\psi_{\vec{k}}(\vec{r} + \vec{l}) = \exp(i\vec{k}_n\cdot\vec{l})\ \psi_{\vec{k}}(\vec{r}) \ . \tag{3.5}$$

That is, the state $\psi_{\vec{k}}$ satisfies the Bloch condition as if it had the wavevector $\vec{k}_n$. Therefore, to describe the total electronic structure of a crystal, only the reduced wavevectors $\vec{k}_n$ need to be considered.

The Schrödinger equation is solved by the variation method. A trial wavefunction $\psi(\vec{k})$ is expressed as a linear combination of normalized basis functions $\phi(\vec{k}_n)$ which satisfy the crystal boundary conditions and the Bloch conditions

$$\psi(\vec{k}) = \sum_n c_n\ \phi(\vec{k}_n) \ . \tag{3.6}$$

The explicit expression for a particular $\phi(\vec{k}_n)$ is given by Koelling and Arbman (2). Substitution of Eqn. 3.6 into

the Schrödinger equation (Eqn. 3.7)

$$H\,\psi(\vec{k}) = E\,\psi(\vec{k}) \tag{3.7}$$

yields

$$\sum_{nm}\sum c_n c_m \langle \phi(\vec{k}_n) | H | \phi(\vec{k}_m) \rangle = E \sum_{nm}\sum \langle \phi(\vec{k}_n) | \phi(\vec{k}_m) \rangle \tag{3.8}$$

Minimization of E with respect to the set of coefficients $c_1, c_2, \ldots c_n$ results in the expression

$$\sum_{n} c_n (H_{nk} - S_{nk}E) = 0; \quad k = 1, 2, \ldots n \tag{3.9}$$

where, $H_{nk} = \langle \phi(\vec{k}_n) | H | \phi(\vec{k}_k) \rangle$

and $S_{nk} = \langle \phi(\vec{k}_n) | \phi(\vec{k}_k) \rangle$.

The coefficients c_n, and thus the wavefunctions, eigenvalues, and eigenvectors, are determined by solving the n simultaneous equations, i.e., the standard eigenvalue problem (4).

For discussions of bonding interactions in the solid, the charge density

$$\rho(\vec{r}) = \psi^*\psi \tag{3.10}$$

is of interest. The density of states, which is the number of electron states in an energy interval, is given by

$$N(E) = \frac{2\Omega}{(2\pi)^3} \sum_{n} \int d^3\vec{k}\,\delta[E_n(\vec{k}) - E] \tag{3.11}$$

where, Ω is the unit cell volume and n is the band index. The integral is evaluated by the method of Gilat and Raubenheimer (5) and applied by Jepsen and Anderson (6).

The knowledge of the components of the eigenvectors permits the decomposition of the total charge density into percentage character from various ℓ-components within the muffin-tin sphere and in turn, partial ℓ-densities of states throughout the Wigner-Seitz cell (1). Similarly, the partial e_g (d_{z^2} and $d_{x^2-y^2}$) and t_{2g} (d_{xy}, d_{yz}, and d_{zx}) densities of states of the metal $\ell=2$ charge density component may be obtained. Summation of the partial densities of states yields the total density of states.

Computational Details for ScS

Hartree-Fock-Slater charge densities for the constituent atoms in their groundstates were calculated utilizing a Herman-Skillman (7) program. The crystal potential of the muffin-tin shape was approximated by the superposition of spherically symmetric atomic potentials, calculated from the atomic charge densities by the method described by Mattheiss (8). The atoms were located at their respective positions in the NaCl lattice according to the convention: the metal atoms occupied the sub-lattice containing the origin and the nonmetal atoms

occupied the sublattice displaced from the origin by $(\frac{1}{2},\frac{1}{2},\frac{1}{2})$.

Wavefunctions and eigenvalues were calculated for 89 k-points in 1/48th of the Brillouin zone of the fcc ScS cell using a basis set of 100 functions. The k-points chosen were those used for a similar calculation for fcc Cu (9). The resulting energy bands (ten in the energy range -1.0 to 1.0 Ry) were fitted by a least squares method to a Fourier series which was truncated to 40 symmetrized plane waves. From the fitted function, the eigenvalue at any k-point within the Brillouin zone could be estimated. The input parameters necessary for the LAPW calculation of ScS are given in Table 3.1.

Table 3.1. Input parameters for the LAPW band structure calculation for ScS[a]

Lattice parameter	9.81146 a.u. (5.192 Å)[b]
Sc muffin-tin sphere radius	2.47649 a.u.
S muffin-tin sphere radius	2.40030 a.u.
% coverage by muffin-tin spheres	51
Energy parameters[c]	
Sc (positive eigenvalues)	0.50
S (positive eigenvalues)	0.23
Sc, S (negative eigenvalues	-0.62

[a]Units used in the calculation: 1 Rydberg (Ry) = 13.605 eV, 1 a.u. = 0.529171 Å.

[b]This work.

[c]The energy parameter used in constructing the radial part of the basis functions (2).

RESULTS

The Band Structure

The energy eigenvalues obtained at k-points of high symmetry within the Brillouin zone for each of the ten bands, are plotted versus the reduced wavevector to obtain the band structure shown in Fig. 3.1 for ScS. The constant potential in the region between muffin-tin spheres defines the zero of energy. Three energy regions may be identified, namely: the single low-lying band (-0.671 to -0.596 Ry) which is composed predominantly of sulfur s-atomic states (Fig. 3.2a) and is referred to as the s-band; the three bands in the energy region -0.019 to 0.255 Ry are essentially sulfur 2p-atomic states (Figs. 3.2b-3.2d) and are referred to as the p-bands or the valence band; the five bands in the energy region 0.382 to 0.776 Ry, which are dominated by metal 3d-states (Figs. 3.3a-3.3e) are referred to as the d-bands or the conduction band. The nine valence electrons per formula unit of ScS fill the lowest four bands, leaving one electron per formula unit to occupy the fifth band. The Fermi level (E_F, the energy of the highest occupied state) falls within the conduction band at 0.5245 Ry.

The remaining band (Fig. 3.2e), which is unoccupied, is an admixture of various atomic states including a

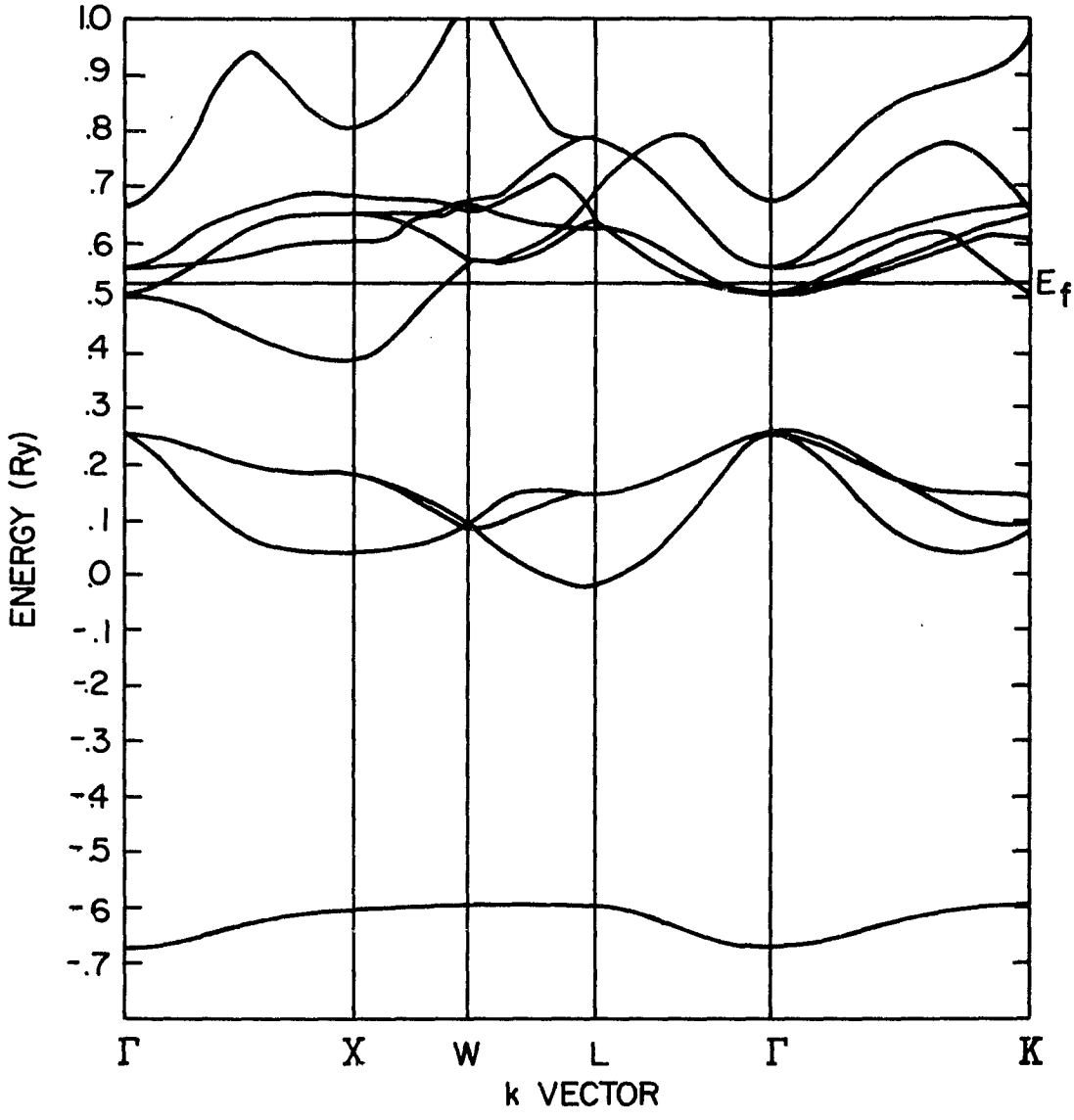

Fig. 3.1. Energy bands of ScS

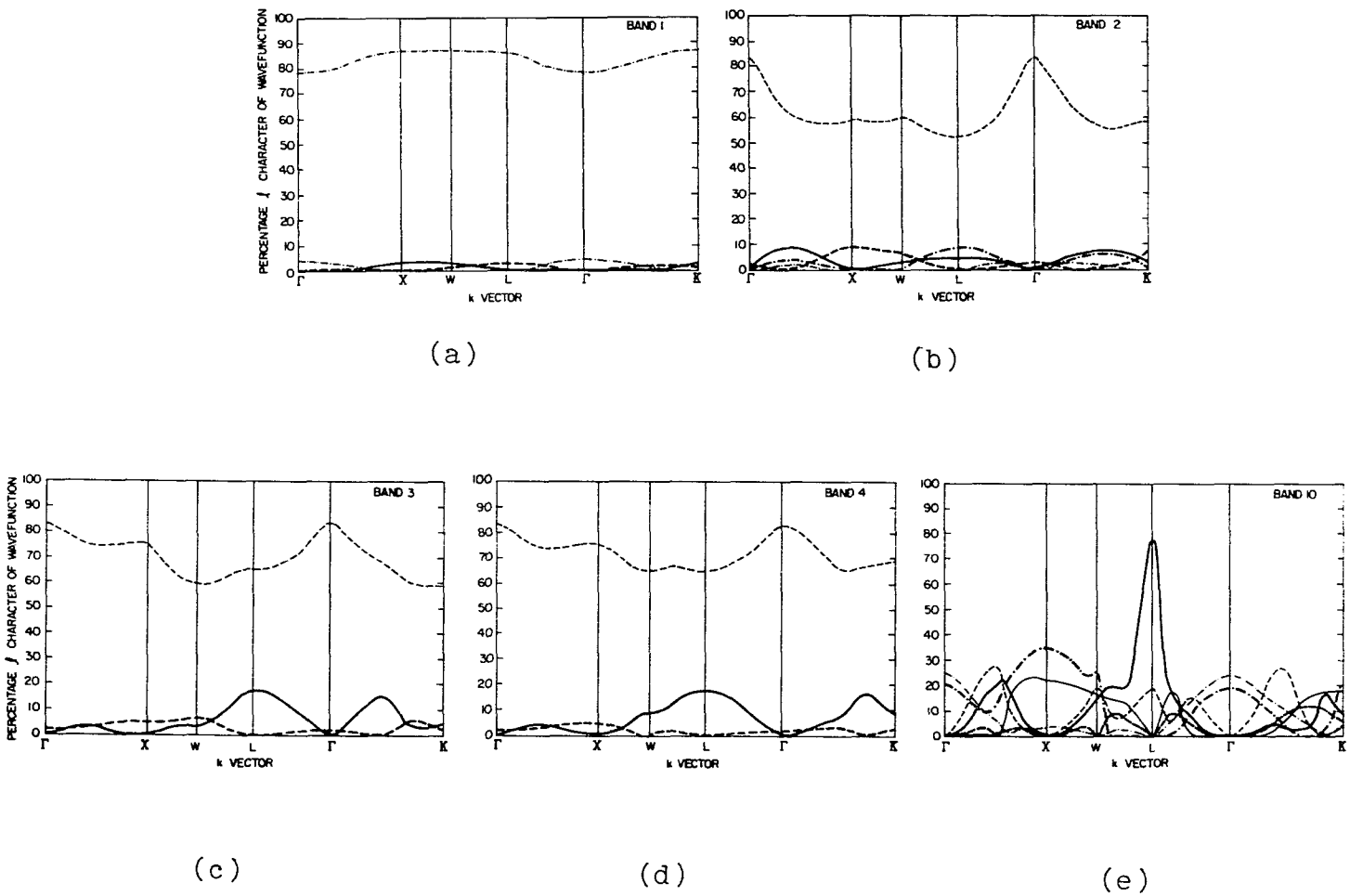

Fig. 3.2. ℓ-Decomposition for bands 1-4, and 10 inside the Sc (thick line) and S (thin line) muffin-tin spheres (ℓ = 0 states: -•-•-•-; ℓ = 1 states: -----; ℓ = 2 states: ———)

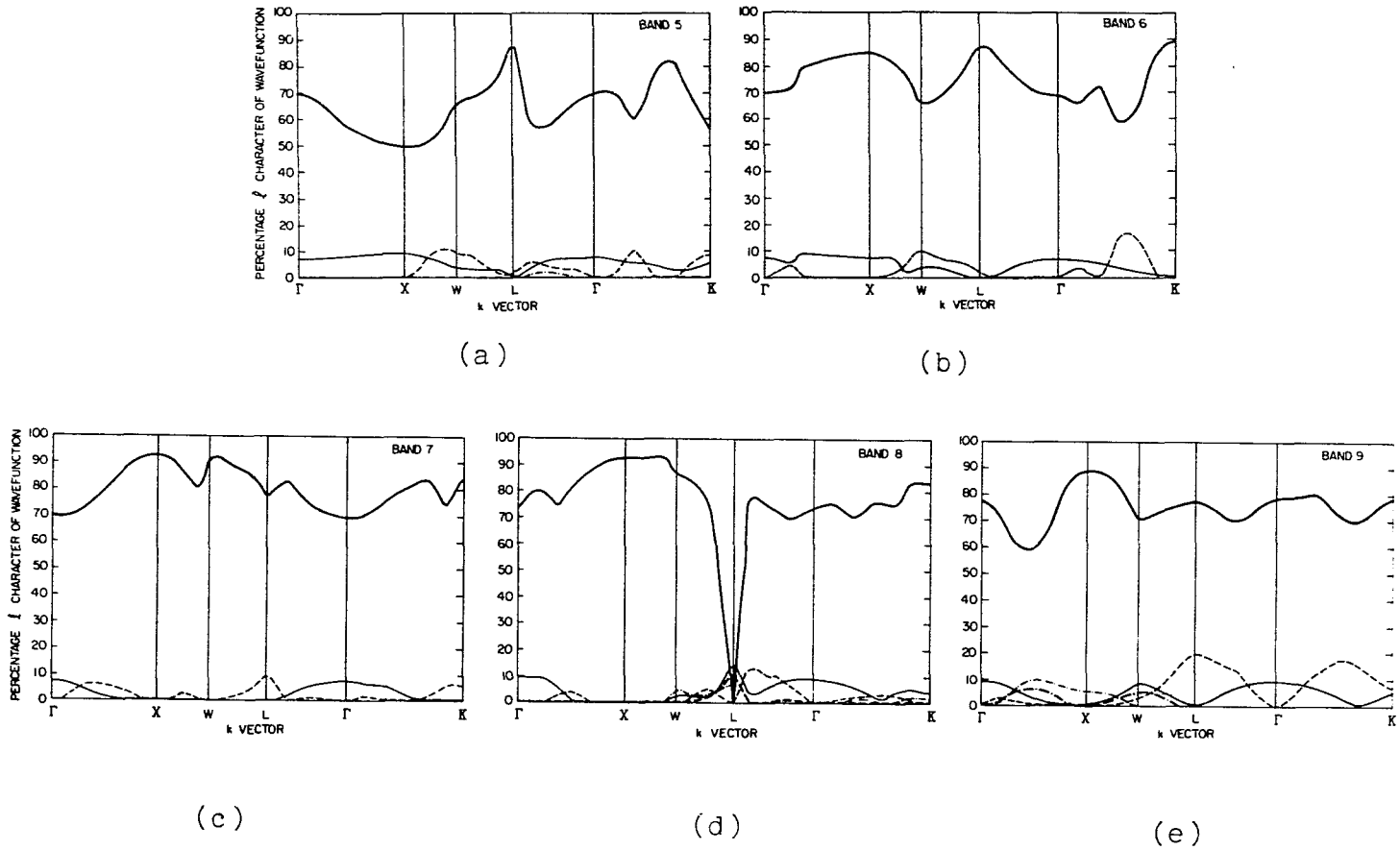

Fig. 3.3. ℓ-Decomposition for bands 5-9 inside the Sc (thick line) and S (thin line) muffin-tin spheres (ℓ = 0 states: -•-•-•-; ℓ = 1 states: -----; ℓ = 2 states: ———)

significant percentage of metal 4s-states. The band model usually given for pure transition metals includes significant overlap of metal 4s and 3d-states in the valence band. However, the interaction between the nonmetal 2s and metal 4s-states in a compound such as ScS, tends to shift the metal 4s-states to higher energy relative to the pure metal. In a molecular orbital interpretation, the nonmetal 2s and metal 4s-states become bonding and anti-bonding bands, respectively. The interaction of metal and nonmetal s-states has also been observed in other MX compounds of the NaCl-structure type by Neckel, et al. (10).

The calculated band structure correctly predicts metallic conductivity for ScS (11) as a result of the occupied states within the conduction band. The occupied states are at the bottom of the conduction band, however, and according to the rigid band approximation, the result of introducing Sc vacancies into the solid is to lower E_F, possibly below the conduction band. In this way, metallic conductivity would be predicted for phases in which Sc/S > 0.666 and the phase Sc_2S_3 (Sc/S = 0.666) would be predicted to be a semiconducting phase. This trend has been observed experimentally (11,12).

The Density of States and Charge Density

The total density of states (including bands 1-9 only) of ScS and the partial ℓ-densities of states (Sc and S, ℓ = 0, 1, 2) are shown in Fig. 3.4. The S s-states, S p-states, and Sc d-states are shown to be the major contributors in the s-band, valence band, and conduction band, respectively.

The Sc d density of states may be further decomposed into the contributions from e_g-like (d_{z^2}, $d_{x^2-y^2}$) and t_{2g}-like (d_{xy}, d_{yz}, d_{zx}) states (Fig. 3.5). The character of the d-states in the valence band is primarily e_g-like, whereas both e_g and t_{2g} states occupy the conduction band. The occupied region of the conduction band consists only of t_{2g} states, however.

Analogies may be drawn between the above treatment of a metal in a NaCl-type crystal structure and a molecular orbital treatment of a metal ion octahedrally coordinated to ligands. (See for example, Cotton and Wilkinson (13)). For a free metal ion, the molecular orbitals which are mainly of metal character, form a bonding and antibonding set of e_g levels and a bonding t_{2g} level which is stabilized in energy relative to the e_g antibonding level by an amount Δ. Similarly, e_g bonding and antibonding and t_{2g} bonding states are formed in the fcc crystal. However, the levels are no longer discrete but rather form broad bands, in

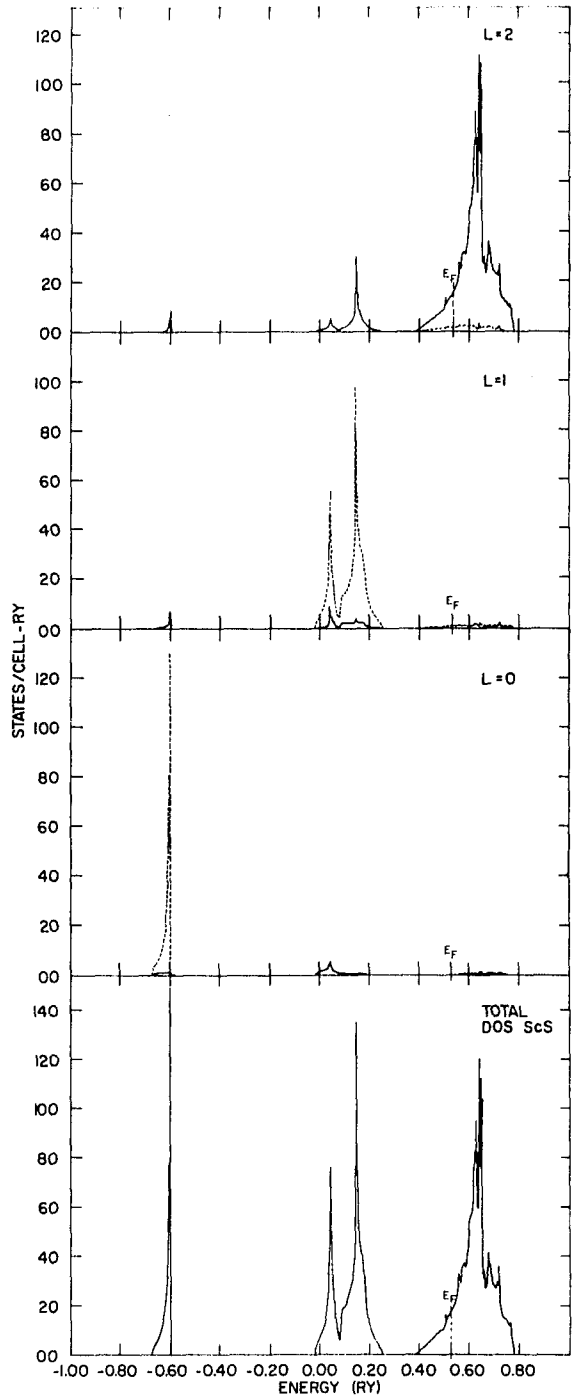

Fig. 3.4. Total density of states (DOS) and partial ℓ-densities of states for ScS (Sc: ——: S: ----)

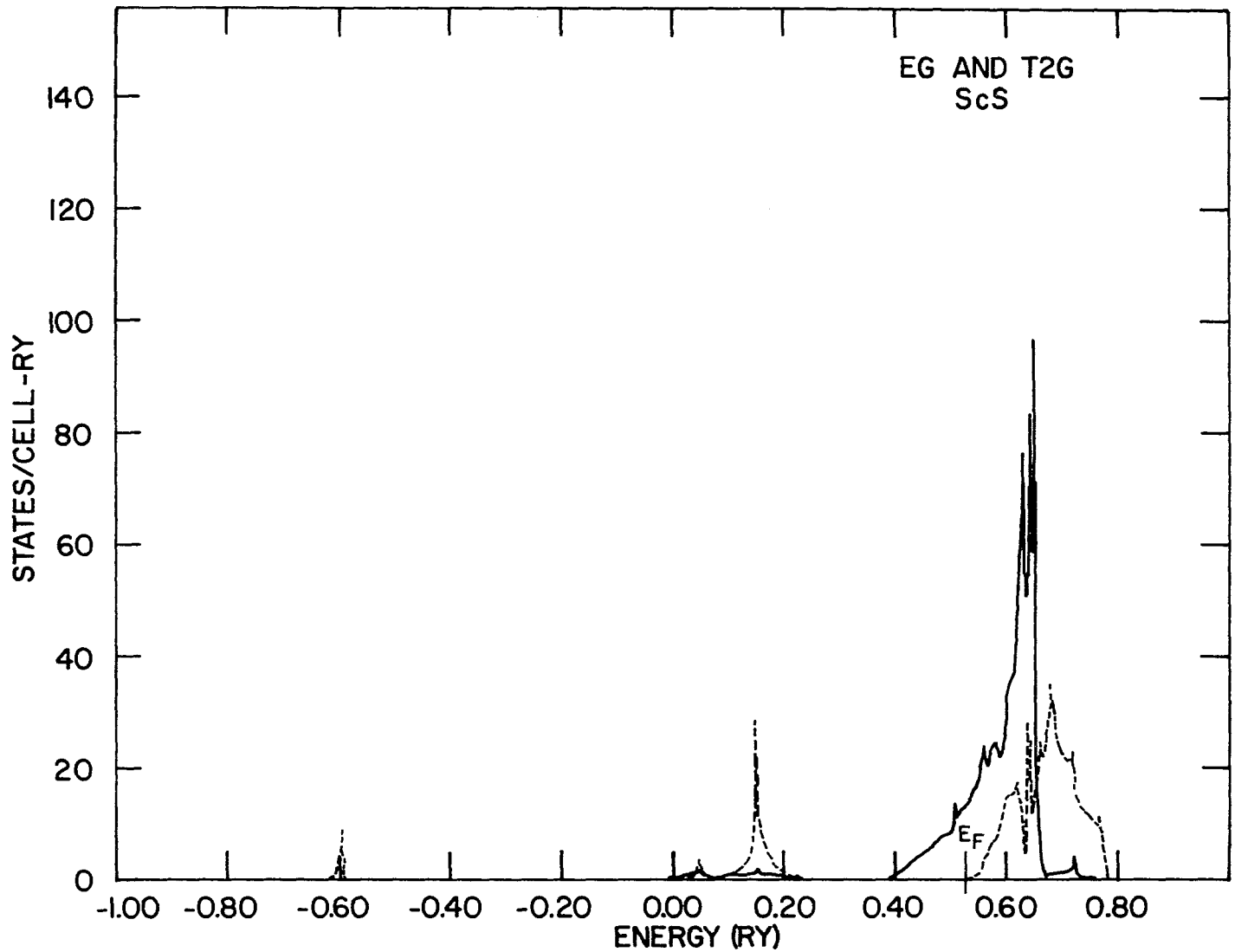

Fig. 3.5. Decomposition of the Sc d-partial density of states into e_g (----) and t_{2g} (——) contributions

which case the t_{2g} bonding and e_g antibonding states overlap rather than have an energy separation Δ.

The average value of the square of the crystal wavefunctions ($\psi^*\psi$) within the muffin-tin sphere, i.e., the charge density of electronic distribution, is useful in determining the directional nature of the bonding. The charge densities which result from the Sc (Fig. 3.6) and S (Fig. 3.7) states within the energy ranges of the s, p, and occupied d-bands, respectively, were evaluated in the 100 plane which passes through the center of the respective muffin-tin sphere. The arrow in each figure points in the specified direction and corresponds to the direction denoted on the projection of the 100 face of a ScS unit cell (shown in the upper right of each figure). The number, located near the point of maximum charge density in each figure, is the value of the charge density (electrons/a.u.^{2}) at the intersection of the direction vector and the muffin-tin sphere boundary.

The maxima in the charge densities of the s- and p-bands of Sc (Fig. 3.6a and 3.6b) occur in the Sc-S direction (100). These results suggest that the orbitals centered at Sc sites participate in σ-bonding with orbitals centered at S sites. The charge densities within the S muffin-tin sphere from states in the s- (not shown) and p-bands (Fig. 3.7a) are essentially symmetric, i.e., they indicate

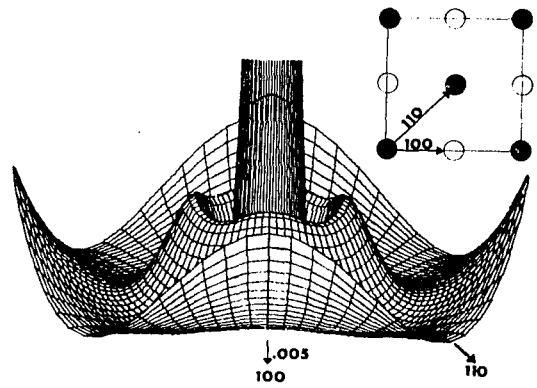

(a)

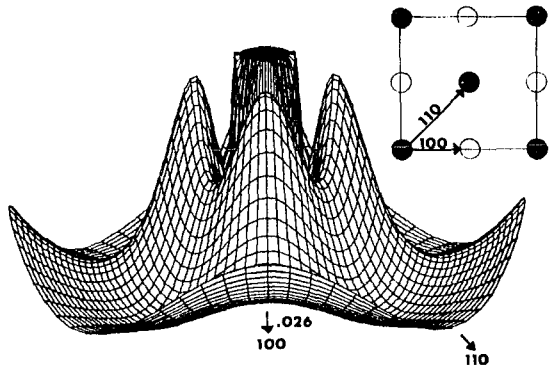

(b)

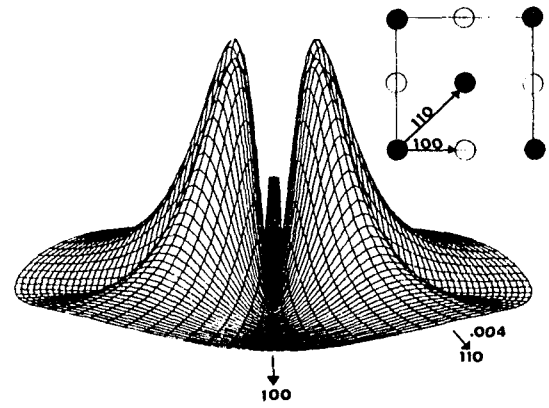

(c)

Fig. 3.6. Charge density in the plane 100 inside the Sc muffin-tin sphere; (a) includes all states in the s-band; (b) includes all states in the p-band; (c) includes all states in the occupied d-band

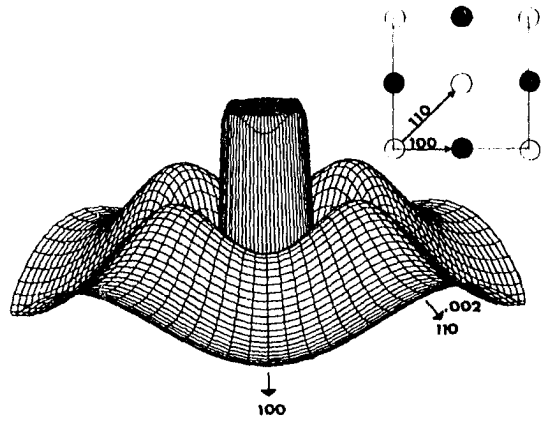

(a)

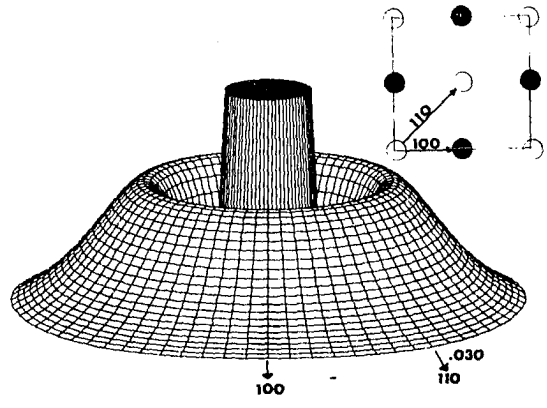

(b)

Fig. 3.7. Charge density in the plane 100 inside the sulfur muffin-tin sphere; (a) includes all states in the p-band; (b) includes all states in the occupied d-band

no preferred bonding direction. The states contributing to the s- and p-bands are primarily S s- and p-states and Sc p- and d-(e_g) states (Fig. 3.4) and further demonstrate the role of metal-nonmetal σ-bonding in these bands.

The maxima of the charge densities within the muffin-tin spheres of Sc (Fig. 3.6c) and S (Fig. 3.7b), as a result of occupied d-states, occur in the 110 direction, suggestive of Sc-Sc σ-bonding or Sc-S π-bonding. Moreover, it is shown that the d-band is composed of metal d (t_{2g}) (Fig. 3.5) and nonmetal p-states (Fig. 3.4), a result which would also predict metal-metal σ-bonding and metal-nonmetal p π-bonding.

Summarizing, the bonding interactions in ScS are described as metal-nonmetal s σ-bonding in the s band, metal-nonmetal p σ-bonding in the valence band (p band), and metal-metal σ-bonding and metal-nonmetal p π-bonding in the conduction band (d band). The magnitudes of the charge densities of Sc and S states in the various bands are given in Table 3.2. The largest proportion of charge density results from states in the valence band, thus the major bonding interaction in ScS is the metal-nonmetal p σ-bonding of the valence band region. The metal-nonmetal p σ-interaction is interpreted as covalent bonding. The charge densities along the 100 direction of Sc and S are

Table 3.2. Magnitudes of the maximum charge densities (electrons/a.u.^{2}) at the muffin-tin sphere radii

	Sc	S
s-Band	0.005	0.003
Valence band	0.026	0.030
Conduction band	0.004	0.002

plotted (Fig. 3.8) to demonstrate the sharing of electronic charge, a feature of covalent bonding.

A rigid band interpretation applied to ScP would predict that E_F would fall at the top of the valence band, i.e., no occupied conduction band states. The ca. 12 kcal enhancement in stability of ScP over ScS (See Section II), in accord with the interpretation, would suggest that the t_{2g}-like states of the conduction band are slightly antibonding in ScS. This agrees with the interpretation of Neckel et al. that the p- and d-bands formed in other NaCl-type compounds could be thought of as bonding-antibonding p-d bands (10).

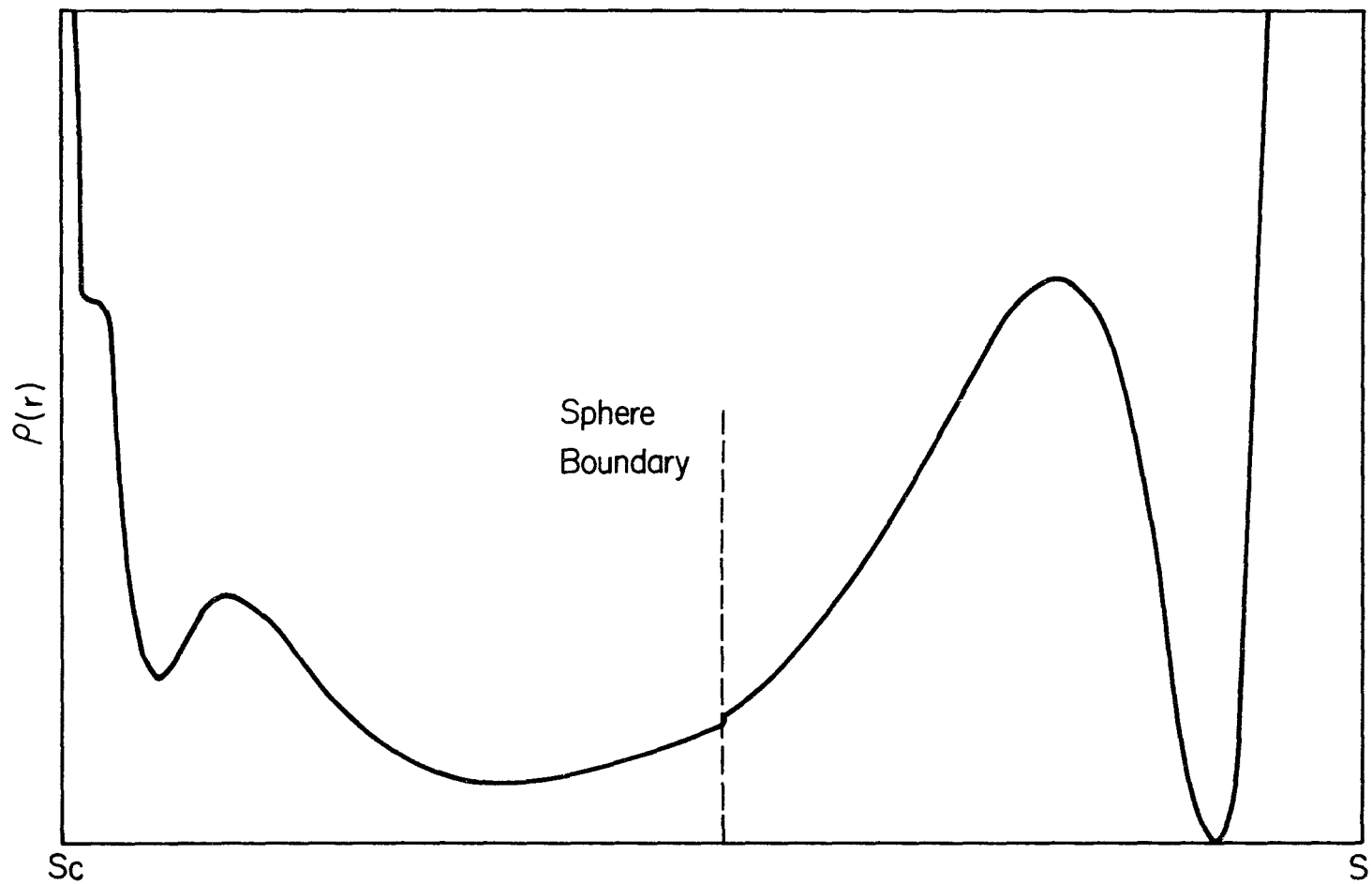

Fig. 3.8. The charge densities of Sc and S muffin-tin spheres along the 100 direction

DISCUSSION

Neckel *et al.* (10,14) have calculated APW band structures and partial densities of states for a series of MX compounds crystallizing in the NaCl-type structure (M = Sc, Ti, V; X = C, N, O) and have noted trends upon changing the metal or the nonmetal atoms. As has been described for ScS, the bonding in these compounds also includes metal-nonmetal p σ-interactions in the valence band and metal-metal σ- and metal-nonmetal p π-interactions in the conduction band.

One criterion for classifying these materials might be in terms of the amount of metal-metal bonding. It appears, however, that for NaCl-type compounds, metal-metal bonding will occur as long as there are occupied states in the conduction band. In the series above, including ScS, ScN would be the only material which would not exhibit metal-metal bonding since E_F in that compound falls at the top of the valence band, *i.e.*, there are no occupied states in the conduction band.

From the results of Neckel *et al.* (10,14), it is observed that the effects of increasing the valence-conduction band gap are as follows: the proportion of metal d-states in the valence band decreases and the character of the d-states changes from a mixture of e_g and t_{2g} states to

predominantly e_g states; the proportion of nonmetal p-states in the conduction band decreases as well; also, the antibonding metal e_g-states in the conduction band are shifted to higher energy. The following interpretation may be applied to these observations. The overlap of the valence and conduction bands allows for increased mixing of the metal d- and nonmetal p-states, thus leading to an enhancement of both metal-nonmetal p σ- and π-bonding. On the other hand, a separation of the valence and conduction bands leads to the localization of the nonmetal p and the metal e_g states in the valence band and the metal t_{2g} states in the conduction band. The localization of states, in effect, seriously reduces the metal-nonmetal p π-bonding.

However, the effect of the valence-conduction band gap may be somewhat counterbalanced by the number of valence electrons available to occupy various states. For example, the valence and conduction bands overlap slightly in ScN, but E_F is so low that the metal t_{2g} states are not populated. The reverse case is also possible; for example, the valence-conduction band gap in VO is 0.12 Ry (14), however, E_F falls at a sufficiently high energy that antibonding nonmetal p-states are occupied, thus allowing for metal-nonmetal p π-type interactions.

The trends associated with changing metal or nonmetal atoms in an MX compound of the NaCl-type structure are

summarized in Fig. 3.9, where the s, valence and conduction bands are represented by blocks of the appropriate widths. Substitution of a more electronegative nonmetal (N with O or S with O) has the effect of narrowing the valence band and increasing the gap between the valence and conduction bands. The effect of substituting a different metal atom is less profound. As a result of substitutions across the series, Sc to V (10,14), and down the period Sc to Y (Fig. 3.9), the valence band is raised to slightly higher energy and the valence-conduction band gap is decreased proportionately. More importantly, E_F is raised in energy as the atomic number of the metal atom is increased.

In summary, an important feature which differentiates between binary compounds crystallizing in the NaCl-structure seems to be the p-d π-interactions which are enhanced by overlapping valence and conduction bands and E_F of sufficient energy to populate the metal t_{2g} and nonmetal p-states in the conduction band. One would predict that p-d π-interactions would be least important in a compound formed by a very electronegative nonmetal and a metal with a small number of valence electrons.

It has been suggested (15) that the metal-d nonmetal-p interactions near the Fermi level (mainly p-d π-type) are of importance for superconductivity. This idea is supported in the scandium-sulfur system. Superconductivity is

observed in $Sc_{1-x}S$, $x \leq 0.10$ (16,17). In a rigid band model, the effect of the scandium deficiency would be to depopulate the p-d π-type states. As shown in Fig. 3.4, the density of nonmetal p-states in the conduction band is lowest at the bottom of the band.

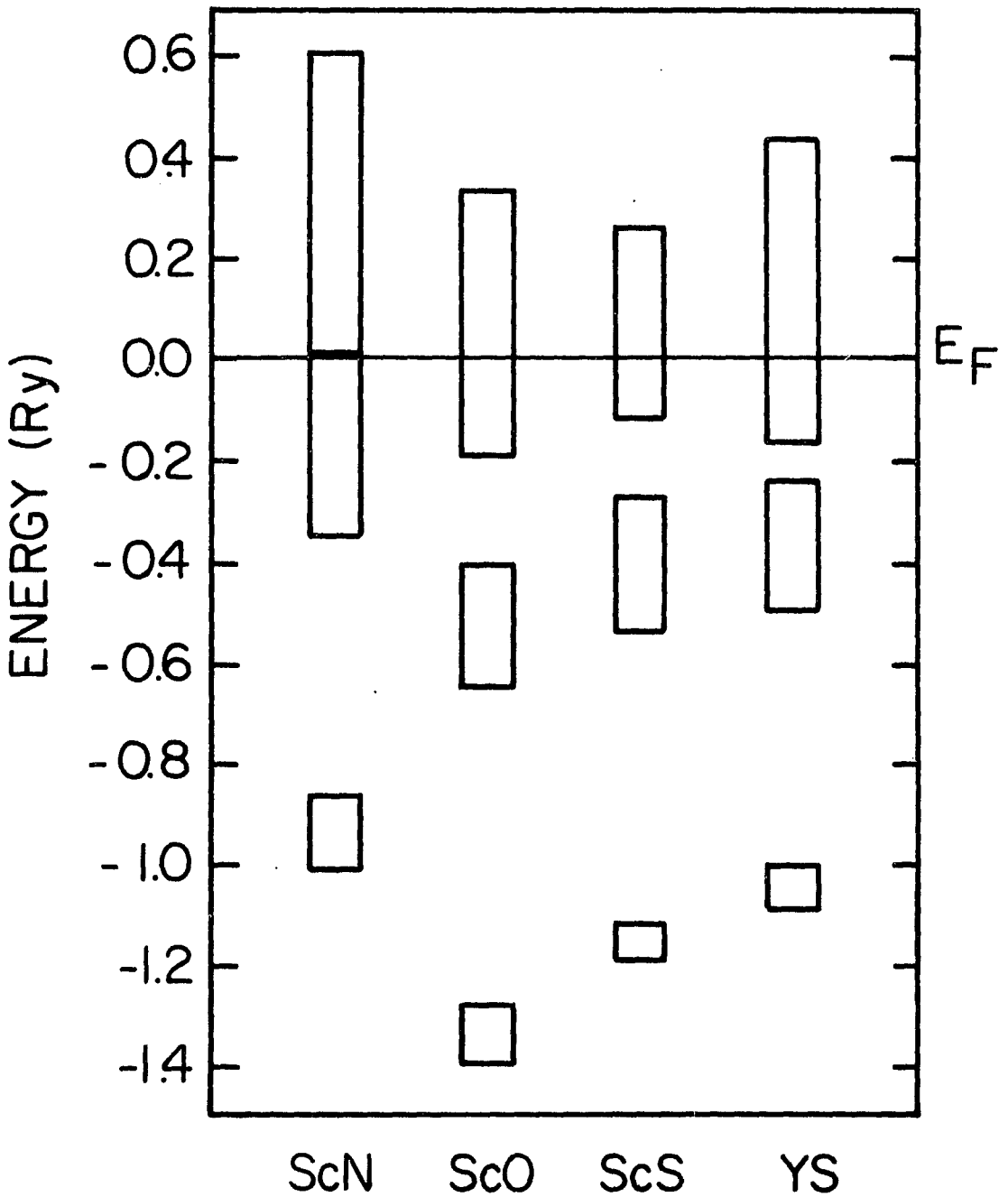

Fig. 3.9. A block representation of the s, p (valence) and d (conduction) bands of a series of NaCl-type compounds. The Fermi level (E_F) is adjusted to zero for convenience.

(ScN, ScO: Ref. 14; YS: Ref. 18; ScS: this work)

REFERENCES

1. Nguyen, T.-H. Ph.D. Dissertation, Iowa State University, Ames, IA, 1980.

2. Koelling, D. D.; Arbman, G. O. J. Phys. F: Metal Phys. 1975, 5, 2041.

3. Loucks, T. "Augmented Plane Wave Method"; Benjamin: New York, 1967.

4. Garbow, B. S.; Dongara, J. J. "Eispack Package", Argonne National Laboratory, Applied Mathematics Division, Technical Memorandum No. 250, 1975.

5. Gilat, G.; Raubenheimer, L. J. Phys. Rev. 1966, 144, 390.

6. Jepsen, O.; Anderson, O. K. Solid State Comm., 1971, 9, 1763.

7. Herman, F.; Skillman, S. "Atomic Structure Calculations"; Prentice-Hall: Englewood Cliffs, NJ, 1963.

8. Mattheiss, L. F. Phys. Rev. 1964, 133, 184.

9. Burdick, G. A. Phys. Rev. 1963, 129, 138.

10. Neckel, A.; Schwarz, K.; Eibler, R.; Weinberger, P.; Rastl, P. Ber. Bunsenges Phys. Chem. 1975, 79, 1053.

11. Dismukes, J. P.; White, J. G. Inorg. Chem. 1964, 3, 1220.

12. Dismukes, J. P. J. Phys. Chem. Solids 1971, 32, 1689.

13. Cotton, F. A.; Wilkinson, G. "Advanced Inorganic Chemistry"; Interscience: New York, 1962; Chapter 26.

14. Neckel, A.; Rastl, P.; Eibler, R.; Weinberger, P.; Schwarz, K. J. Phys. C: Solid State Phys. 1976, 9, 579.

15. Schwarz, K. J. Phys. C: Solid State Phys. 1977, 10, 195.

16. Narayan, P. B. V.; Finnemore, D. K. J. Less-Common Metals 1978, 61, 231.

17. Moodenbaugh, A. R.; Johnston, D. C.; Viswanathan, R. Mat. Res. Bull. 1974, 9, 1671.

18. Schwarz, K.; Wimmer, E. J. Phys. F: Metal Phys. in press.

SECTION IV. XPS AND UPS MEASUREMENTS OF DEFECT SCANDIUM MONOSULFIDE

INTRODUCTION

The core-electron and valence-conduction band spectra of cubic $Sc_{1-x}S$ over the concentration range $0.0 \leq x \leq 0.2$ were obtained by X-ray (XPS) and ultraviolet (UPS) photoelectron spectroscopy. The valence-conduction band spectra are compared to the theoretical valence density of states (DOS) for ScS which was discussed in Section III.

A comparison is also made between the Sc and S core-electron binding energies (XPS) in $Sc_{1-x}S$ and in other sulfides and scandium compounds to deduce the character of the Sc-S bond in $Sc_{1-x}S$. XPS measurements of Sc_2S_3, Sc_2O_3 and Sc metal were completed and included in this comparison.

The Sc 2p core levels in the cubic defect monosulfides were found to exhibit an unusual satellite structure. This prompted a complete analysis of the positions and relative intensities of the satellite to fundamental peaks in the Sc 2p energy region as a function of x by a least squares curve fitting procedure. The results are discussed in relation to a model proposed for similar satellite structure noted in the W 4f region of cubic Na_xWO_3.

THEORY AND METHOD

The Measurement and Spectrometer

Einstein was the first to recognize the photoelectric effect whereby a material exposed to a quantum of radiation will emit photoelectrons (1). It was not until the 1950s, however, that the analysis of the photoelectron energies was found useful in qualitative identification of the elements (2) and that the measured core electron binding energies were found to be dependent upon the chemical environment (3). Siegbahn, et al. (3) are credited with introducing the technique of XPS, also known as ESCA (Electron Spectroscopy for Chemical Analysis) as a viable chemical tool. Various sources have been used for the exciting radiation, typically, Al (1486.6 eV), or Mg (1253.6 eV) Kα, in which the spectra are referred to as XPS, or HeI (21.2 eV), and HeII (40.8 eV) radiation, for which the spectra are referred to as UPS. A more complete description of XPS and UPS may be found in Carlson (4) and Fadley (5) and will be summarized below.

In the photoelectron spectroscopy experiment, a sample material is exposed to a flux of nearly monoenergetic radiation with an average energy hν and the kinetic energy of the resulting photoelectrons is observed. The energy conservation equation for the most simple photoemission process is

$$h\nu = E_b^F(k) + E_{kin} + \phi_{(sample)} \qquad (4.1)$$

where $E_b^F(k)$ is the binding energy of the k^{th} electron state referred to the Fermi level E_F, i.e., the energy required to excite an electron from the k^{th} energy level to E_F; E_{kin} is the kinetic energy of the electron; and ϕ_{sample} is the sample work function, i.e., the energy required to remove an electron from E_F to the vacuum level. For a real measurement, thermodynamic equilibrium of a spectrometer in electrical contact with a metallic sample requires that the Fermi levels of the sample and spectrometer be equal. The emitted photoelectron then adjusts to the spectrometer work function ϕ_{spec}, a constant for a given spectrometer, and has a kinetic energy E_{kin}^{meas}, where the relationship between E_{kin} (Eqn. 4.1) and E_{kin}^{meas} is

$$E_{kin} + \phi_{sample} = E_{kin}^{meas} + \phi_{spec}. \qquad (4.2)$$

Substitution of Eqn. 4.2 into Eqn. 4.1 gives the result

$$E_b^F(k) = h\nu - E_{kin} - \phi_{spec}. \qquad (4.3)$$

The spectrometer work function ϕ_{spec} may be determined by measuring the binding energy using a standard material, e.g., Au $4f_{7/2}$ level, and defining ϕ_{spec} as the energy difference between the measured and accepted values. In this way, the information required for determination of the binding energy of the k^{th} electron level of a conducting material may be obtained. Other methods must be used for nonconducting samples (see Refs. 4,5).

A schematic of the photoelectron spectrometer used in this study is shown in Fig. 4.1. A narrow energy band of photoelectrons is focused onto a collector slit by a double focusing hemispherical electrostatic analyzer and detected by an electron multiplier of the channeltron type. As the voltage applied to the analyzer and lens system is swept, an energy spectrum of the emitted photoelectrons is obtained. The signal, i.e., the intensity of photoelectrons having a particular kinetic energy value, may be amplified by a rate meter, as shown in the figure, or averaged by repeatedly scanning the appropriate energy range, collecting the data in a computer, as used in this study, and subsequently recording the spectrum on an x-y recorder.

The escape depth for photoelectrons with kinetic energies in the range of several keV is 20-30 Å which implies that photoelectron spectroscopy is a surface technique. A rule of thumb is that at a residual pressure of 10^{-6} torr, oxygen (assuming a sticking coefficient of unity) will deposit on a sample surface at the rate of one monolayer per second. Therefore, spectrometer pressures in the range of 10^{-9} torr are necessary before meaningful information about the bulk material may be inferred.

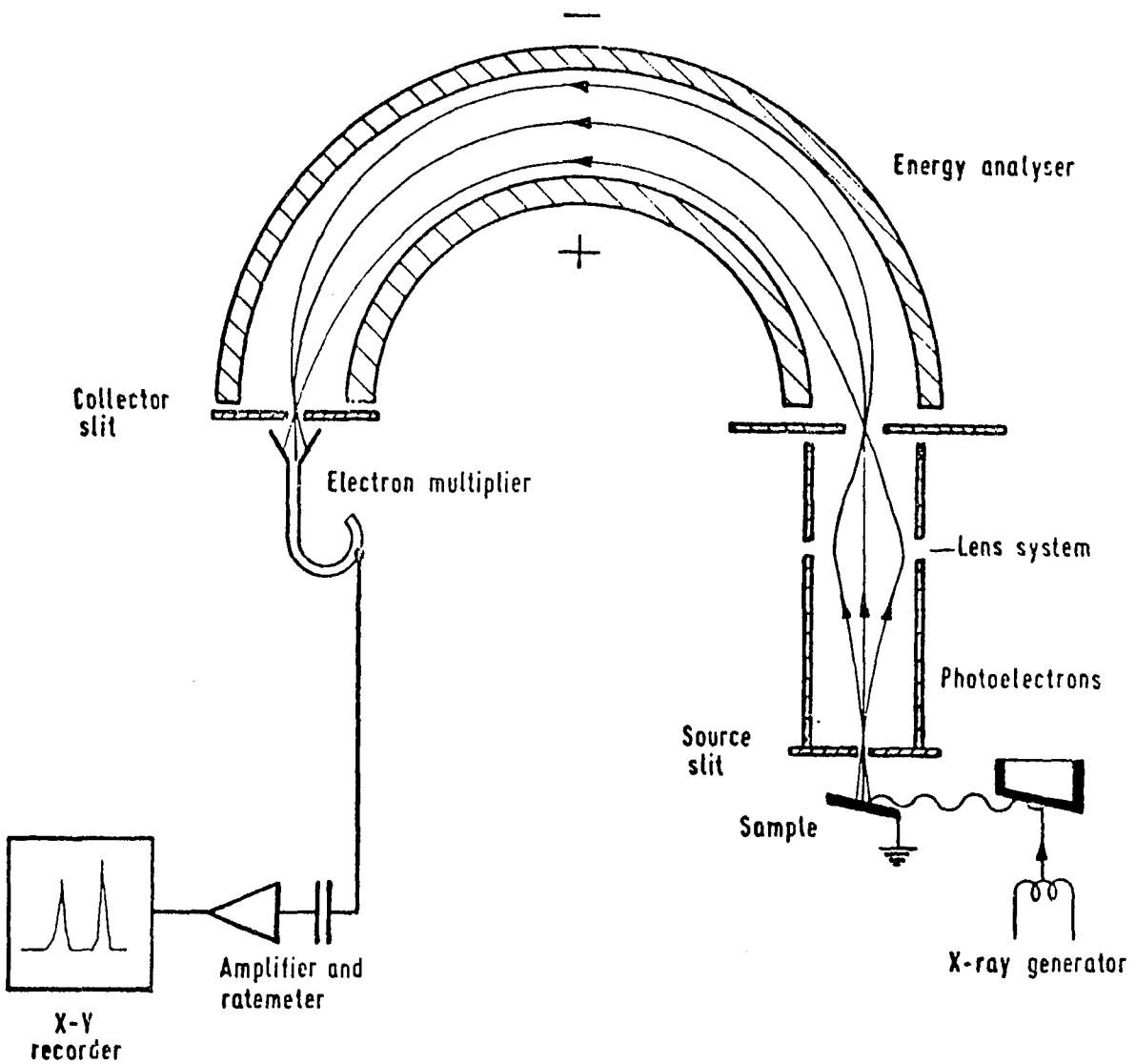

Fig. 4.1. Schematic of the AEI ES200 photoelectron spectrometer (Ref. 6)

Interpretation of Photoelectron Spectra

The aim of an XPS (or UPS) measurement is to determine the positions, intensities, and shapes of peaks in the energy spectrum. There is a one-to-one correspondence between the observed photoelectron peaks and the molecular orbitals in any material being measured. Since core-electron states are atomic-like, core binding energy determination provides a means for elemental analysis. The binding energy of the k^{th} peak is the energy difference between an initial neutral state and a final state with one electron removed, and is a function of the relative shielding of electrons in the k^{th} electron level from the nuclear charge, i.e., the chemical environment.

The peak intensity is proportional to the quantity of element present; however, it is also a function of the photoelectric cross-section, defined as the transition probability for exciting an electron system from an initial state ψ_i to a final state ψ_f with a known incident photon flux (dependent upon the radiation source).

Factors which affect the peak width include: broadening as a result of the inherent energy width of the exciting radiation (nonmonochromatized Al Kα ∿1 eV; He I ∿ 0.2-0.3 eV) and the resolving capability of the spectrometer, or broadening as a result of sample charging, sample inhomogeneities, or the superposition of chemically shifted peaks.

The peak shape and width are also dependent upon final state effects resulting from an electron core hole (see Ref. 7). A few examples of final state effects are: (1) Spin-orbit splitting: an initially filled core state with one electron removed has two possible final states corresponding to a spin-orbit coupling parameter J=L+S, L-S. The intensity of each component is proportional to 2J+1. (2) Inelastic scattering: photoelectrons which undergo inelastic collisions in the sample before being analyzed. This will appear as a high background at the high binding energy side of a primary peak. (3) Multiplet splitting: coupling of a hole in a metal core level with an unfilled d valence level. (4) Shake-up: an electron in a valence state which is promoted to an excited state as a result of energy transfer from the photoelectrons. (5) Plasmons: the collective oscillation, with frequency ω_p, of conduction electrons in a metallic phase as a result of energy transfer. The final state effects (3)-(5) all result in satellite structure at the high binding energy side of the primary peak.

In other words, the XPS spectrum yields relative final state energies directly, but it is the task of the spectroscopist to interpret its meaning.

Valence Band Spectra

Either an X-ray or UV photon source may be used to excite valence electrons to obtain a valence-conduction band spectrum. The experimentally determined spectrum is related to the valence density of states (DOS) which can be calculated from the band structure (Section III). It can be shown that the XPS valence band spectrum, corrected for inelastic scattering, is more reliable than the UPS valence band spectrum in reproducing the shape of the DOS, with appropriate photoelectron cross-sections considered (8). The resolution of the He I UPS line is significantly narrower than the XPS line ($\sim$1 eV); however, the UPS valence band is more sensitive to surface and final state effects (4,8).

EXPERIMENTAL

Sample Preparation

Various compositions of scandium sulfide were prepared by direct combination of the elements as described in Section I. The initially reacted Sc_2S_3 and a metal-rich two phase mixture were contained in W crucibles and were homogenized at 1200 and 1300°C, respectively, in high vacuum. The compositions $Sc_{1-x}S$ ($0.0 \leq x \leq 0.2$) were obtained by heating the metal-rich material intermittently and removing a small portion of the residue from each heating for XPS measurement. The residue was characterized by following the weight loss after each heating (assumed to be primarily Sc) and the lattice parameter, which was determined from X-ray powder diffraction measurements. The high purity Sc metal used in this study was in the form of an electropolished sheet obtained from Ames Laboratory. All materials were handled in a N_2 recirculating dry box during preparation and between heatings to reduce the exposure to oxygen.

XPS and UPS Measurement

The XPS and UPS measurements were made in an AEI ES200B spectrometer equipped with a standard Al Kα X-ray source (1486.6 eV) and He I UV lamp (21.2 eV) and coupled to a

Nicolet 1180 computer for data collection and signal averaging. The powdered sulfide samples were pressed into In sheets which, in turn, were mounted onto a Ag metal strip inside a recirculating He dry box (H_2O, $O_2 \leq 0.5$ ppm) attached to the spectrometer. The internal calibrants to the energy scale were Ag $3d_{5/2}$ at 368.0 ± 0.2 eV and Au $4f_{7/2}$ at 84.0 ± 0.2 eV (9) (FWHM = 0.8 eV with Al Kα). Spectra were recorded in an ultrahigh vacuum chamber with a residual pressure of $2 \cdot 10^{-9}$ torr or less for all levels accessible with the radiation used, including Sc, S, C, and O levels. The two latter species were the result of surface contamination. Spectra were recorded both before and after surface cleaning by argon ion etching. Etching reduced the C 1s and O 1s signals but did not significantly change either the positions or shapes of the Sc or S peaks in Sc_2S_3 and in the defect scandium monosulfides; however, etching narrowed the Sc metal peaks considerably. Sample charging did not occur for these samples.

XPS measurements were also obtained from high purity Sc_2O_3 and Sc_2O_2S (prepared by reaction of stoichiometric amounts of Sc_2S_3 and Sc_2O_3 at 600°C). These insulating materials were powdered and mounted on scotch tape covered Ag strips. Binding energies were referenced to either C 1s (tape) or to $Sc_{0.8}S$ which was homogeneously mixed with the

powdered material before measurement, since the oxide peaks shifted as a result of sample charging.

Typically, a region of 12.5 or 25 eV was scanned 30-40 times at a scan speed of 2.0 eV/sec. and the results were stored in the computer at 0.05 eV/channel.

Spectra of the valence-conduction band regions of the sulfides and the Sc metal were obtained utilizing both Al Kα and He I radiation. It was necessary to average several hundred scans of the 0-25 eV region when Al Kα radiation was used, and 10-20 scans when He I radiation was the exciting source.

Curve Fitting Procedure

The multiple peaks of the Sc 2p core level spectra in $Sc_{1-x}S$ ($0.0 \leq x \leq 0.2$) were approximately fitted to two sets of spin-orbit split peaks, where the spin-orbit splitting (4.7 eV) and the intensity ratio of $2p_{3/2}$ to $2p_{1/2}$ (2.69/1.00) were obtained from a similar fitting technique applied separately to the $2p_{3/2}$ and $2p_{1/2}$ peaks in the Sc_2S_3 spectra. The fitting procedure was accomplished by the use of the computer program APES (Analyzed Photoelectron Spectrum) (10) which first smoothes the experimental data, corrects for a nonzero baseline and inelastic scattering, then fits the corrected spectra with a linear combination

of Gaussian and Cauchy functions by a nonlinear least squares technique. The program allows for the variation of the peak heights, positions, and full widths at half-maximum (FWHM) for up to four spin-orbit doublets with fixed spin-orbit splitting and intensity ratio.

This fitting procedure is not unique nor is it capable of reproducing the spectra exactly; however, the parameters used seemed to give a reasonable and consistent set of peak positions and widths for the satellite and primary peaks in the Sc 2p spectra throughout the composition range.

RESULTS AND DISCUSSION

The Valence-Conduction Band

The valence band XPS (Al Kα) and UPS (He I) spectra of $Sc_{1.01}S$ and the theoretical valence density of states (Section III) in ScS, which is convoluted with a 1.1 eV half-width Gaussian function but not adjusted for photoelectron cross-section effects, are shown in Fig. 4.2. The energy scale is relative to $E_F = 0.0$ eV. The peaks at 5.0 eV and 14.0 eV in the XPS valence band spectrum may be principally ascribed to the S 3s and 3p levels in the solid, respectively, by comparison to the theoretical DOS curve.

The Sc d-band appears as a small shoulder on the low energy side of the S 3p level in the XPS spectrum. The S 3p and Sc 3d levels are more clearly resolved in the UPS spectrum relative to the XPS valence band. The fact that the S 3s level does not appear in the UPS valence band is presumably a result of the low photoelectric cross-section of s-levels with He I radiation (11). The theoretical DOS, however, does not correctly predict the position of the S 3p level relative to the Fermi level. A self-consistent band calculation should give closer agreement.

The valence-conduction region was followed as a function of x in cubic $Sc_{1-x}S$. The effect of shifting the Fermi level

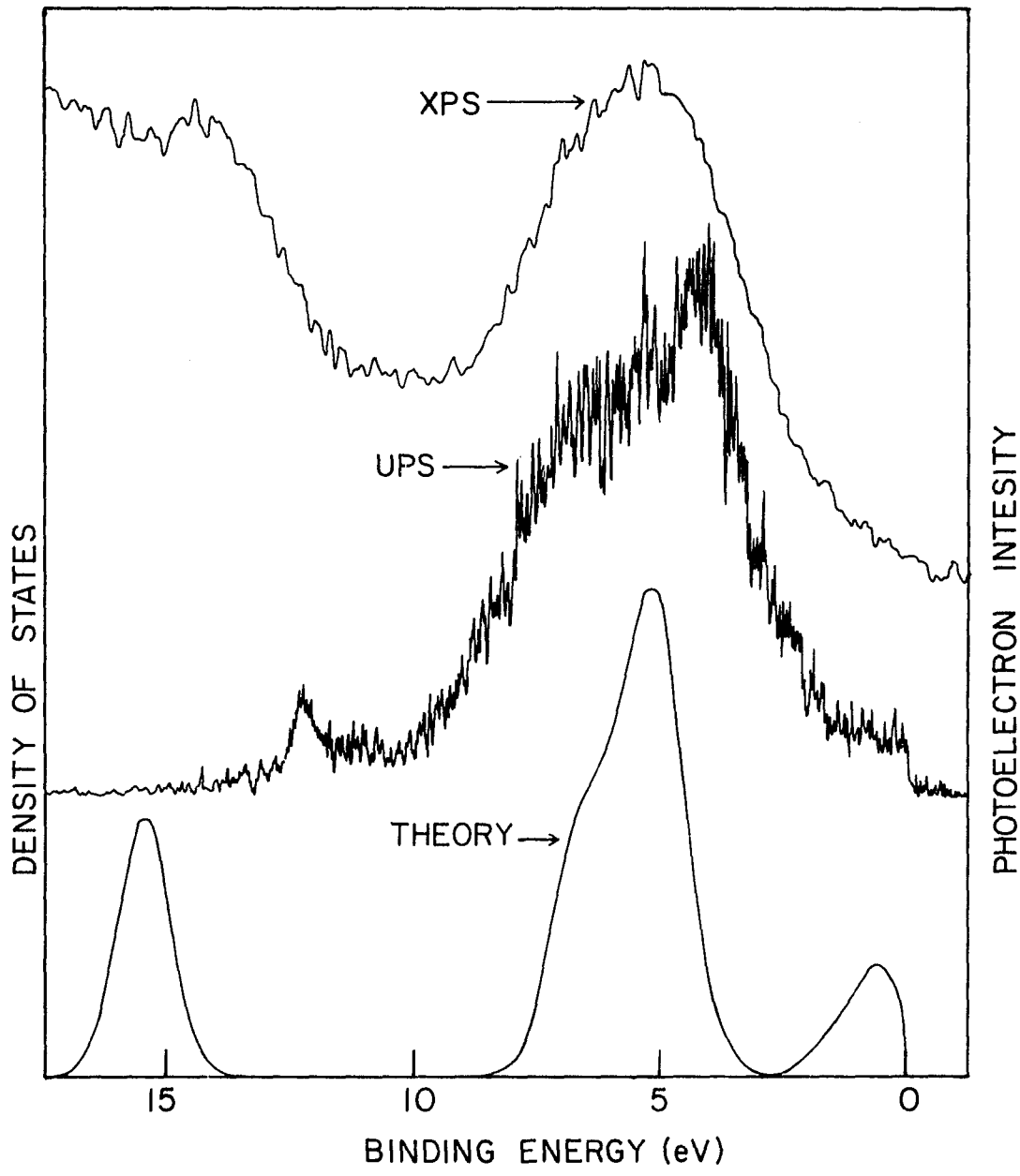

Fig. 4.2. The XPS and UPS spectra of $Sc_{1.01}S$ and the valence density of states in ScS convoluted with a 1.1 eV half-width Gaussian function. The energy scale is relative to E_F = 0.0 eV

with an increased number of conduction electrons ($Sc_{0.8}S \longrightarrow Sc_{1.01}S$) was not measurable.

S 2p Core Levels

The S 2p binding energies in cubic $Sc_{1-x}S$ ($0.0 \leq x \leq 0.2$) and Sc_2S_3 are reported in the last column of Table 4.1. (The S $2p_{3/2}$ and $2p_{1/2}$ levels are not resolvable with non-monochromatic X-rays). The S 2p binding energy of 162.7 eV in $Sc_{1.01}S$ and the slightly lower binding energy of 162.3 in $Sc_{0.81}S$ compare well with the previously reported values (12), with elemental sulfur (13) and with sulfur in other metallic sulfides (12). The S 2p binding energy of 161.7 eV measured in Sc_2S_3 is intermediate between the value reported for ionic (CaS at 161.0, Ref. 12) and more metallic (TiS at 162.3, Ref. 12) sulfides. These results suggest that covalent bonding is significant in the defect monosulfides $Sc_{1-x}S$ ($0.0 \leq x \leq 0.2$), i.e., there is very little charge transfer from metal to sulfur. With increasing concentration of Sc vacancies, however, an ionic bonding component becomes more important, i.e., charge transfer increases, as observed in the decreasing S 2p binding energy from $Sc_{1.01}S$ to $Sc_{0.81}S$ to Sc_2S_3.

Table 4.1. Binding energies of the Sc and S 2p core levels in various compositions of the scandium-sulfur system and in related compounds (eV ± 0.2 eV, referenced to Au $4f_{7/2}$ = 84.0 ± 0.2 eV)

Sc/S	Lattice Parameter	Sc $2p_{3/2}$[a] Peak 1	Peak 2	S $2p_{3/2,1/2}$
1.09[b]	5.179 Å	401.8	398.5	162.4
1.05[b]	5.192 Å	401.8	398.6	162.6
1.03[b]	5.194 Å	402.0	398.8	---
1.01[b]	5.191 Å	401.9	398.9	162.7
0.94	5.186 Å	401.9	398.8	162.5
0.90	5.180 Å	401.8	398.9	162.3
0.81	5.165 Å	401.6	399.0	162.3
Sc_2S_3		401.5		161.7
Sc metal		398.6		
Sc_2O_3[c]		403.2		

[a]The spin orbit splitting is assumed to be 4.7 eV.

[b]Sc/S > 1.00 denotes a metal-rich two phase mixture, ($Sc_{1.00}S$ + Sc metal).

[c]Measured relative to Sc_2S_3.

Sc 2p Core Levels

The XPS spectra of the Sc 2p core levels in Sc metal and in representative scandium sulfides of varying compositions are shown in Fig. 4.3. Two peaks (the spin-orbit doublet $2p_{3/2}$, $2p_{1/2}$) in an approximate ratio of 2:1 are observed in the Sc 2p energy region in Sc metal and Sc_2S_3. The Sc $2p_{3/2}$, $2p_{1/2}$ doublet appears at 398.6, 403.2 eV in the pure metal, in agreement with (14), and at 401.5, 406.2 eV in Sc_2S_3.

A much more puzzling spectrum is obtained for the Sc 2p region in each of the nonstoichiometric monosulfides. Instead of a spectrum consisting of a single spin-orbit doublet, the Sc 2p region is composed of a superposition of at least two sets of spin-orbit doublets separated from each other by 2-3 eV (Fig. 4.3). The Sc 2p region from four two-phase mixtures ($Sc_{1.00}S$ and excess Sc metal) and three defect monosulfides were approximately fitted to two sets of spin-orbit doublets as described previously. The corrected and fitted curves for Sc_2S_3 and $Sc_{0.81}S$ are shown in Figs. 4.4 and 4.5, respectively. The sample composition, lattice parameters, and resulting binding energies for the $2p_{3/2}$ high (Peak 1) and low (Peak 2) binding energy peaks are reported in columns 1-4 of Table 4.1.

The binding energy of Peak 1 is 401.9 in $Sc_{1.01}S$ and decreases to 401.6 eV in $Sc_{0.81}S$, a value very close to the

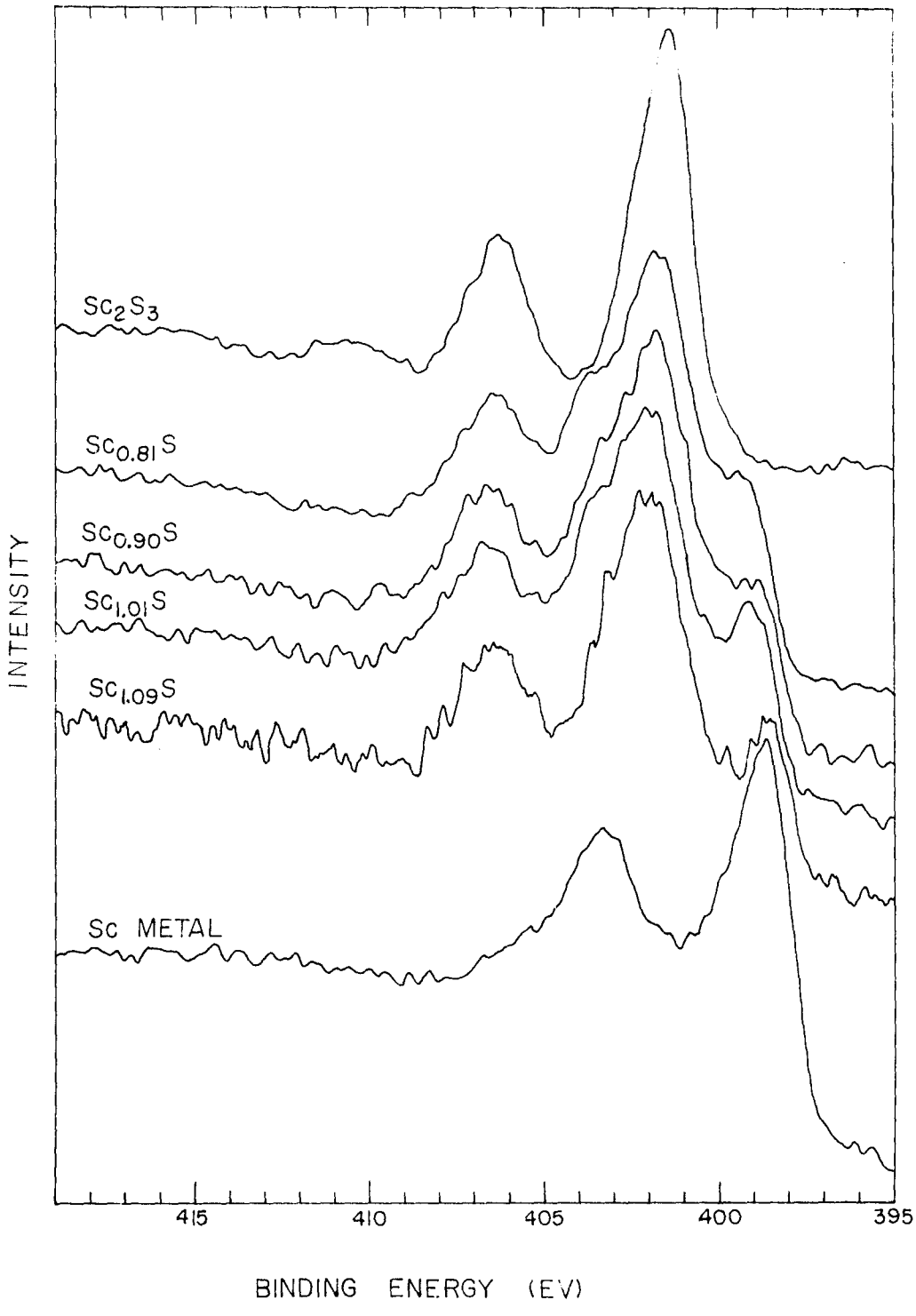

Fig. 4.3. The XPS Sc 2p core spectra of Sc metal, metal-rich and defect scandium monosulfides, and Sc_2S_3

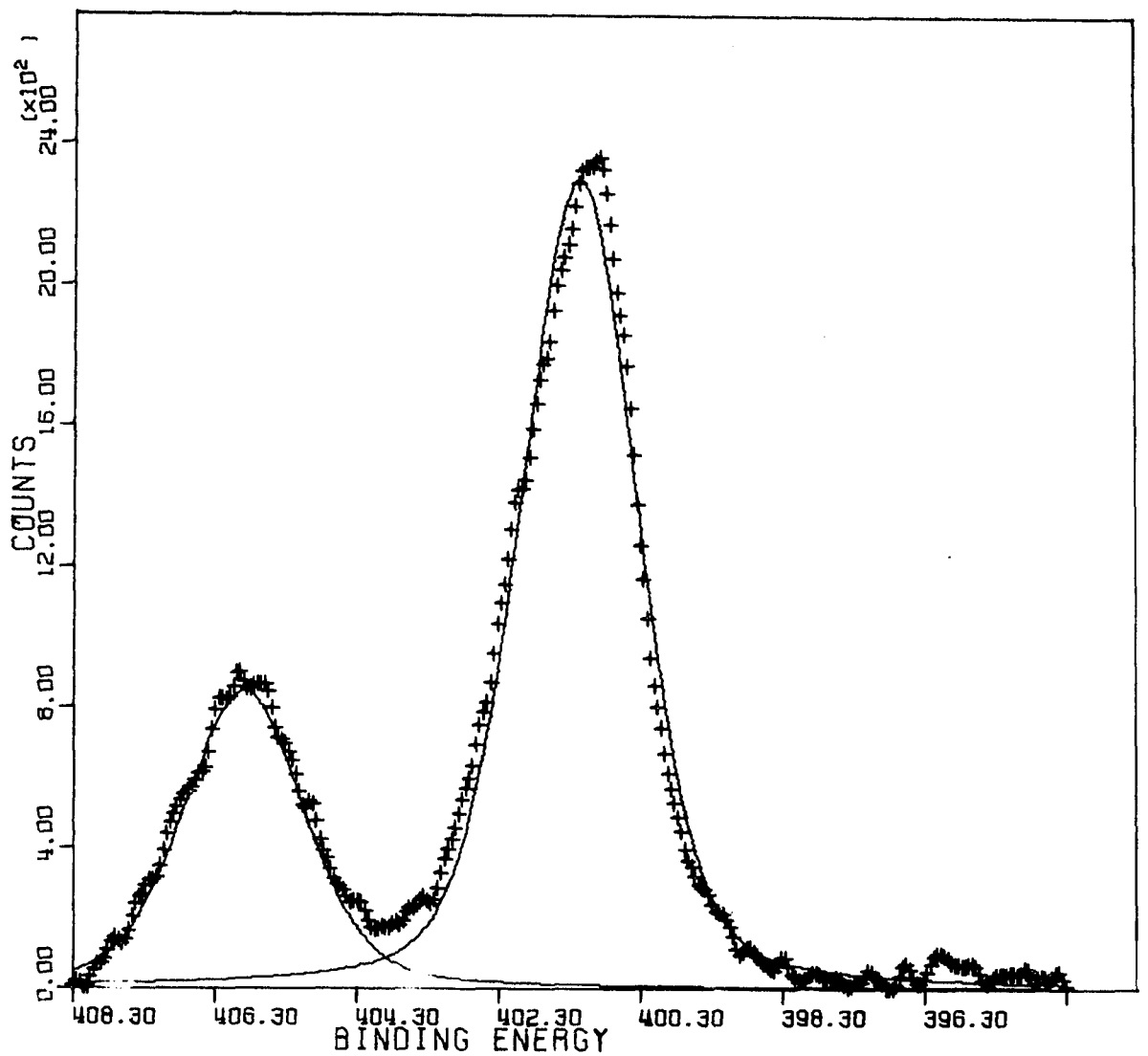

Fig. 4.4. The XPS Sc 2p spectrum of Sc_2S_3 fitted with 1.9 and 2.0 eV FWHM Gaussian-Cauchy functions for the $2p_{3/2}$ and $2p_{1/2}$ peak, respectively.

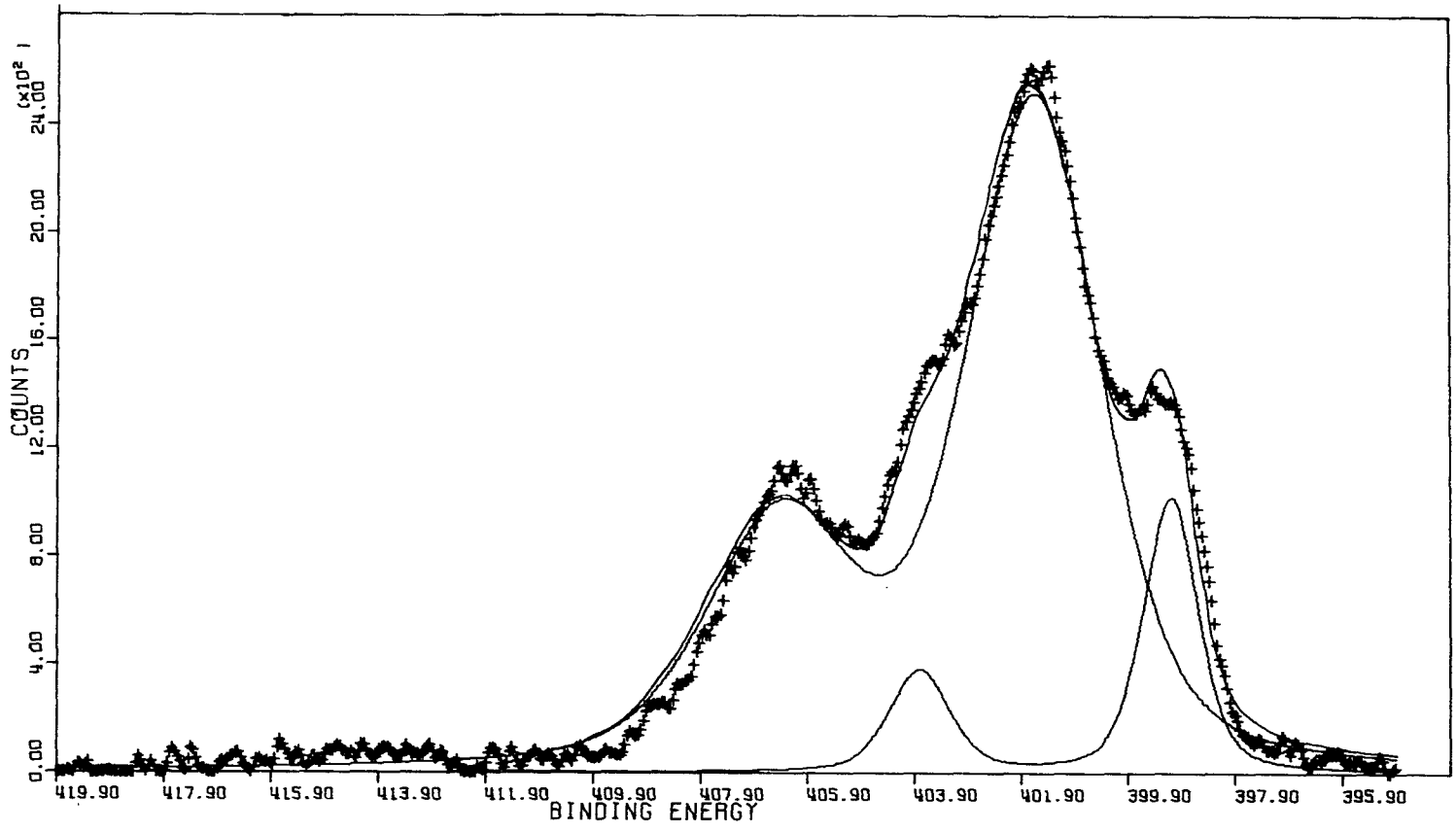

Fig. 4.5. The XPS Sc 2p spectrum of $Sc_{0.81}S$ fitted with two spin-orbit doublets

Sc $2p_{3/2}$ binding energy in Sc_2S_3. The binding energy of Peak 2 in the two phase metal-rich mixtures ($Sc_{1.09}S$ to $Sc_{1.01}S$), not unexpectedly, is 398.5 eV, the same value as the Sc $2p_{3/2}$ binding energy in the pure metal. Contrary to the binding energy of Peak 1 which decreases with decreasing scandium concentration, the binding energy of Peak 2 in the monosulfide homogeneity range increases with decreasing scandium concentration, such that the Peak 2 binding energy is 399.0 eV in $Sc_{0.81}S$. The binding energies of Sc $2p_{3/2}$ (Peaks 1 and 2) and S 2p as a function of scandium to sulfur mole ratio Sc/S are plotted in Fig. 4.6b. Peak 1 is broadened considerably with respect to Peak 2, as seen in Fig. 4.5 and by comparing the average FWHM obtained from the curve fitting procedure (Peak 1, FWHM=2.8 eV; Peak 2, FWHM=1.4 eV).

It is unlikely that the observed Sc 2p spectra are the result of macroscopic sample inhomogeneities, either bulk or surface, since each sample was annealed for several hours at temperature > 1600°C, (Sc_2S_3 decomposes above 1300°C and the vapor pressure of Sc metal at 1600°C is $3 \cdot 10^{-4}$ atm. (15)), thus eliminating bulk inhomogeneities. Also, the XPS measurements were made on finely powdered samples which showed only a single phase X-ray diffraction pattern, not a surface phase of equal or greater intensity than the bulk material.

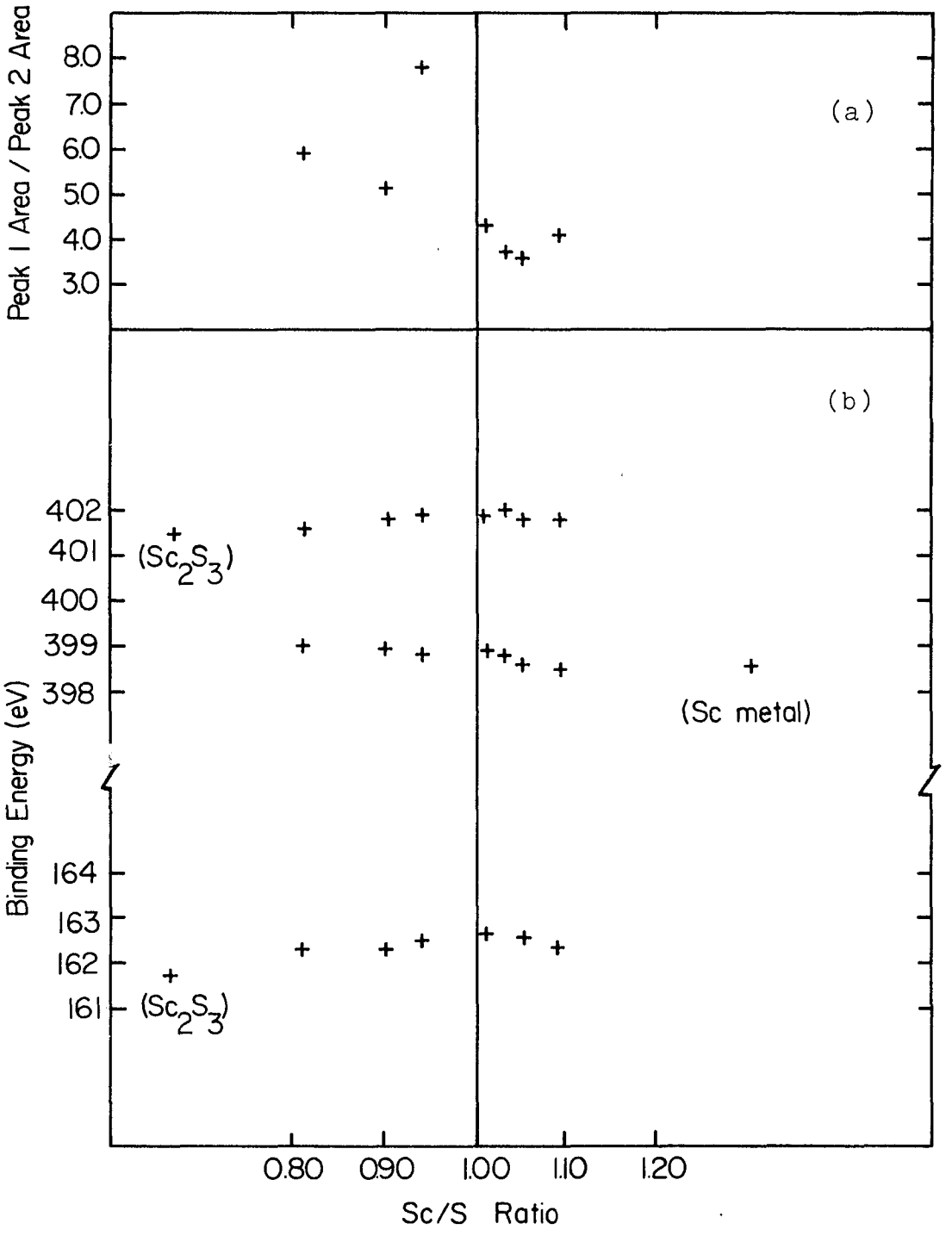

Fig. 4.6. The ratio of Satellite (Peak 1) to fundamental (Peak 2) peak areas (a) and binding energies of Peak 1; Peak 2, and S 2p (b) as a function of mole ratio Sc/S

The only known oxide of scandium Sc_2O_3 (16) and an oxysulfide Sc_2O_2S (17) were also measured by XPS in this study. The Sc 2p spectrum of $Sc_{0.81}S$ mixed with increasing amounts of Sc_2O_3 is shown in Fig. 4.7. The binding energy of Sc $2p_{3/2}$ in Sc_2O_3 is shifted to higher energy by 1.6 eV relative to Peak 1 in $Sc_{0.81}S$, resulting in a value of 403.2 eV which is in agreement with Gimzewski et al. (14). The Sc $2p_{3/2}$ binding energy in Sc_2O_2S, measured relative to C 1s at 285.0 in scotch tape since the sample is non-conducting, is 401.8 ± 0.5 eV which is close to the value of Peak 1 in $Sc_{0.81}S$. However, a shake-up satellite separated from the primary peak by ∿11 eV is observed in the spectra of Sc_2O_3 and Sc_2O_2S whereas it is not observed in any of the sulfides. (The satellite is especially noticeable in a spectrum of Sc_2O_3 after the inelastic scattering correction has been made.) Also, oxygen present in the initial spectrum could be removed by prolonged argon etching with no significant change apparent in the Sc 2p spectrum. Therefore, it seems improbable that oxygen contamination is significant in the $Sc_{1-x}S$ samples.

Finally, the presence of initial Sc^{3+} and Sc^{2+} states (mixed valence) can be refuted. First, the results of Dismukes and White (18) and the band structure results (Section III) suggest that the scandium sulfides should be described as having equivalent Sc sites with a system of

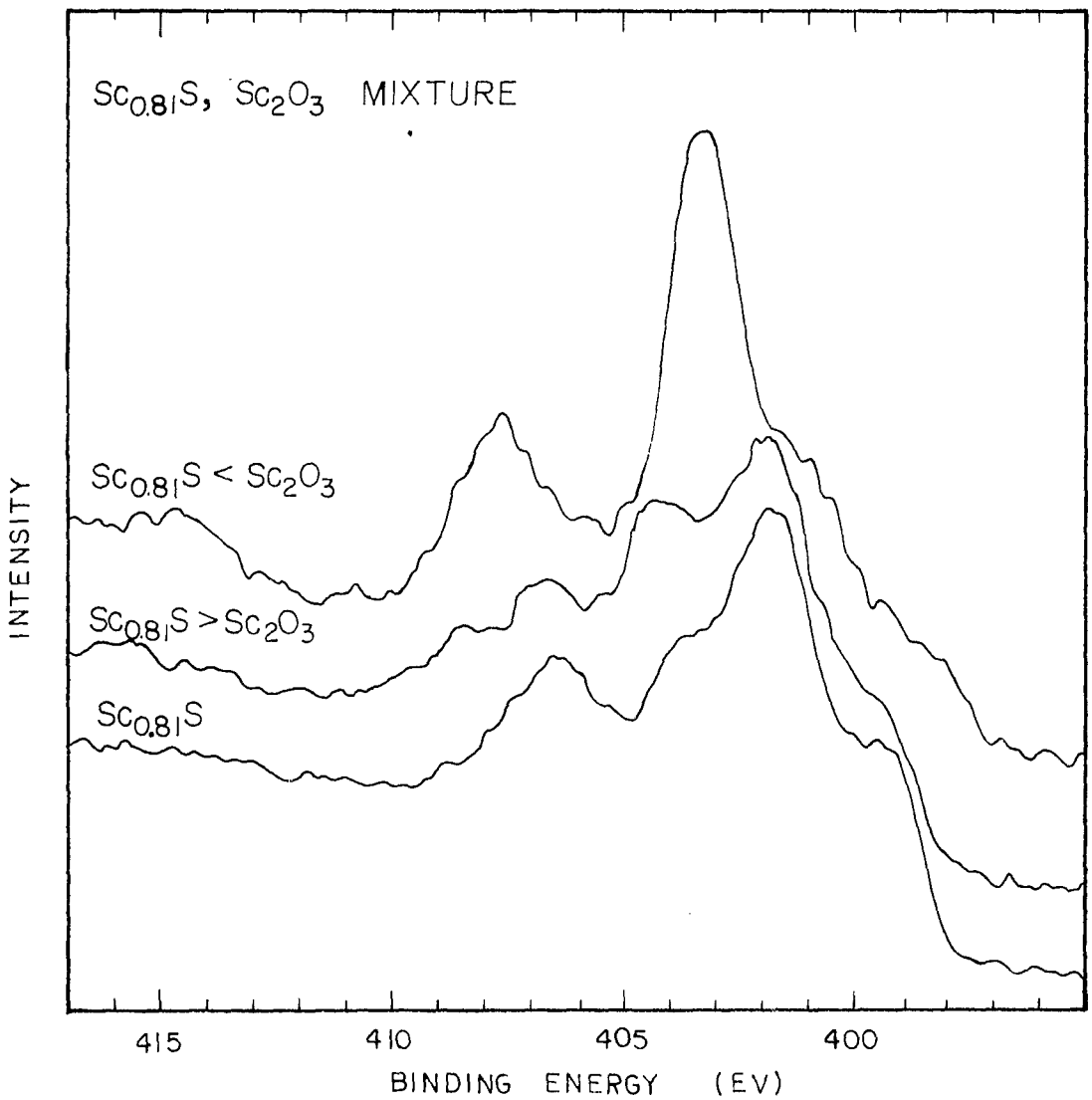

Fig. 4.7. The XPS Sc 2p spectra in pure $Sc_{0.81}S$ and two mixtures of $Sc_{0.81}S$ and Sc_2O_3

delocalized conduction electrons; secondly, the intensity ratios $(Sc^{3+})/(Sc^{2+})$ as a function of composition which are expected (0.0 in $Sc_{1.00}S$; 0.89 in $Sc_{0.81}S$) are inconsistent with the observed ratio of areas Peak 1/Peak 2 (Fig. 4.6a).

In addition, the broadness of Peak 1 compared to Peak 2, and the noticeable binding energy shift of the Sc 2p peaks with changing composition (Fig. 4.6) suggest that the unusual feature is a result of a final state many-body satellite rather than an initial state effect. It also is a localized phenomenon, interacting with scandium energy levels only, since a doubling in the peaks in the 2s, 3s, and 3p Sc regions are also observed, but are not observed in the sulfur levels.

It is also worth noting that of other Sc compounds recently studied in our laboratory by XPS, a single Sc 2p spin-orbit doublet is observed in Sc_2Se_3 (this work) and ScP (19); however, a satellite structure similar to that observed in $Sc_{1-x}S$ is noted in the Sc 2p spectrum in ScSe (this work).

Comparison to Other Inorganic Sc Compounds

XPS studies have been reported on a number of inorganic Sc $(3d^0)$ compounds as systems in which the effect of charge transfer shake-up mechanisms may be studied without interference from multiplet splitting. (Both would result

in a high binding energy satellite in the XPS spectrum (20-23).) Shake-up satellites have been observed at ∿12 eV higher binding energy relative to the primary Sc 2p peak in compounds such as ScF_3 (21,22), $ScBr_3$ (22) and Sc_2O_3 (20-23), and at 8 eV higher binding energy in $Na_3Sc(SO_4)_3 \cdot 5H_2O$ (21). The ∿12 eV satellite is ascribed to a charge transfer excitation of an electron in the nonmetal 2p e_g valence band state to a metal 3d e_g conduction band state ($e_g \rightarrow e_g^*$) (20-23), whereas the ∿8 eV satellite is attributed to a $t_{2g} \rightarrow t_{2g}^*$ transition, e.g., O 2p → Sc 3d t_{2g} (21,23). Frost et al. (21) also suggest that in compounds in which metal-nonmetal π-bonding is significant, satellites resulting from both transitions ($e_g \rightarrow e_g^*$ and $t_{2g} \rightarrow t_{2g}^*$) may occur, with the net result of one very broad satellite which may not be distinguishable from the background. The fact that charge transfer shake-up satellites are not observed in the Sc 2p spectrum of Sc_2S_3 nor in $Sc_{1-x}S$ ($0.0 \leq x \leq 0.2$) would suggest that nonmetal-p metal-d π-interactions are more important in Sc_2S_3 and $Sc_{1-x}S$ than in Sc_2O_3. This is in complete agreement with the band structure results discussed for ScS and ScO in Section III.

The Sc 2p binding energies in $Sc_{1.01}S$ and Sc_2S_3 are compared with those in other Sc compounds in Table 4.2. Peak 2 was selected as the primary peak in $Sc_{1.01}S$ because of its narrowness compared to Peak 1, and by comparison to

Table 4.2. Binding energies of Sc 2p in a series of compounds (eV 0.2 eV; relative to Au $4f_{7/2}$ at 84.0 ± 0.2 eV)

Sample	Sc $2p_{3/2}$	Sc $2p_{1/2}$
Sc metal[a]	398.6	403.2
$Sc_{1.01}S$[a]	398.8	403.2
ScP[b]	399.7	404.5
Sc_2Se_3[a]	401.1	405.7
Sc_2S_3[a]	401.5	406.2
Sc_2O_3[a]	403.2	407.9

[a]This work.

[b]Ref. 19.

the S 2p binding energy which implies covalent rather than ionic bonding in the solid. The monosulfide and monophosphide exhibit Sc 2p binding energies comparable to metallic scandium suggestive of covalent bonding, while Sc_2S_3 and Sc_2Se_3 exhibit binding energies closer to Sc_2O_3, typical of more ionic bonding character. The Sc 2p binding energy in ScP compared to ScS implies less metal-nonmetal p-d mixing in ScP relative to ScS, possibly as a result of one fewer electron per formula unit in the ScP (see Section III). The binding energies of Sc in the series

Se→S→O reflect increased ionic bonding character with increased electronegativity of the nonmetal.

Comparison of $Sc_{1-x}S$ and Na_xWO_3

A visual inspection of a series of defect monosulfides $Sc_{1-x}S$ ($0.0 \leq x \leq 0.2$) and cubic sodium tungsten bronzes Na_xWO_3 ($0.5 \leq x \leq 1.0$) (24) suggests electronic similarities between the two systems. Both materials exhibit a range of vivid metallic colors which are dependent, in one case on Sc concentration and in the other, on Na concentration -- violet at the low concentration range and yellow to gold at the high concentrations, and copper to orange in between. The Na_xWO_3 phases are metallic conductors in the cubic perovskite phase and undergo structural phase transitions to lower symmetry structures as well as becoming semiconducting at low sodium concentrations.

The band structure of $NaWO_3$ (25) consists of a broad valence band which is composed primarily of O 2p states mixed significantly with W 5d states, and a W 5d conduction band in which O 2p states mix appreciably. The states at the top of the valence band and at the bottom of the conduction band are π bonding and antibonding states, respectively (26). The Fermi level falls within the conduction band. A very comparable description was given for the ScS band

structure in Section III. Therefore, it is not necessarily an accident that the materials have similar appearances.

The XPS and UPS of cubic Na_xWO_3 compositions have been examined (27-29) and of special interest is a very intense satellite structure in the W 4f spectra shifted by ∿2 eV from the fundamental peak.

Features of the W 4f satellite and fundamental peaks which warrant consideration with respect to the Sc 2p energy region include the following (29): (1) a numerical analysis of the W 4f data yields a narrow asymmetric fundamental peak and a much broader symmetric peak at ∿2 eV higher binding energy; (2) the intensity ratio (satellite/fundamental) decreases with increasing Na concentration; (3) the energy separation between the satellite and fundamental peak increases with increasing Na concentration. As a result of this remarkable resemblance between the satellite phenomena, as well as the electronic structures of Na_xWO_3 and $Sc_{1-x}S$ (Fig. 4.6), the Na_xWO_3 system is proposed as the model by which to interpret the XPS Sc 2p levels in $Sc_{1-x}S$.

The W 4f satellite structure has been carefully analyzed with respect to two different satellite mechanisms, both of which predict the qualitative features correctly, but neither of which is totally successful alone (28,29). The two mechanisms will be summarized below and their applicability to $Sc_{1-x}S$ will be discussed.

One mechanism proposes that the attractive potential of the core hole which results from the photoelectric process can split off a localized state from the conduction band. The population of the localized state is related to the filling of the initial state and in this case would increase with Sc concentration, as observed. The lower and higher binding energy peaks correspond to the final states in which the localized level is filled (screened) and unfilled (less screened) but broadened as a result of its presence, respectively.

Secondly, a mechanism in terms of a plasmon excitation is proposed. A low energy ($\sim$2 eV) plasmon is a collective excitation of conduction electrons with a frequency ω_p, which in a free electron band model, is proportional to $x^{\frac{1}{2}}$ (x = number of conduction electrons). The binding energy difference between the plasmon satellite peak and the fundamental peak ΔE ($= h\omega_p$) is the excitation energy. Therefore, $\Delta E \alpha x^{\frac{1}{2}}$, as is observed both in Na_xWO_3 ($h\omega_p \simeq 1.7$ eV) and in $Sc_{1-x}S$ ($h\omega_p \simeq 1.9$ eV), is consistent with a plasmon state mechanism. However, neither theory explains all the observed features, as shown by Chazaviel et al. (29).

In conclusion, it is suggested (29) that the proper theory to explain the W 4f satellite phenomenon and possibly the Sc 2p satellite, is most probably intermediate in character.

REFERENCES

1. Einstein, A. Ann. Physik 1905, 17, 32.

2. Steinhardt, R. G.; Serfass, E. J. Anal. Chem. 1953, 25, 697. Steinhardt, R. G.; Granados, F. A. D.; Post, G. I. Anal. Chem. 1955, 27, 1046.

3. Siegbahn, K.; Nordling, C.; Johansson, G.; Hedman, J.; Heden, P. F.; Hamrin, K.; Gelius, U.; Bergmark, T.; Werme, L. O.; Manne, R.; Baer, Y. "ESCA Applied to Free Molecules"; North-Holland: Amsterdam, 1969.

4. Carlson, T. A. "Photoelectron and Auger Spectroscopy"; Plenum: New York, 1975.

5. Fadley, C. S. In "Electron Spectroscopy"; Brundle, C. R.; Baker, A. D., Eds.; Academic: New York, 1978; Vol. 2, Chapter 1.

6. "AEI ES200 Electron Spectrometer Instruction Manual", AEI Scientific, Manchester, England, 1972; Fig. A.1.1.a.

7. Wertheim, G. K. In "Electron Spectroscopy"; Brundle, C. R.; Baker, A. D., Eds.; Academic: New York, 1978; Vol. 2, Chapter 5.

8. Fadley, C. S.; Shirley, D. A. J. Research of Natl. Bur. Stand.-A 1970, 74A, 543.

9. Ebel, M. F. J. Electron Spectrosc. and Rel. Phenom. 1976, 8, 213.

10. Luly, M. H. "APES (Analyzed Photoelectron Spectrum)", Ames Laboratory-USDOE, Ames, IA, May 1979, No. IS-4694.

11. Battye, F. L.; Schulz, H.; Goldman, A.; Hüfner, S.; Seipler, D.; Elschner, B. J. Phys. F: Metal Phys. 1978, 8, 709.

12. Franzen, H. F.; Umaña, M. X.; McCreary, J. R.; Thorn, R. J. J. Solid State Chem. 1976, 18, 363.

13. Swartz, W. E.; Wynne, K. J.; Hercules, D. M. Anal. Chem. 1971, 43, 1884.

14. Gimzewski, J. K.; Fabian, D. J.; Watson, L. M.; Affrossman, S. J. Phys. F: Metal Phys. 1977, 7, L305.

15. Hultgren, R.; Desai, P. D.; Hawkins, D. T.; Gleiser, M.; Kelley, K. K.; Wagman, D. D. "Selected Values of the Thermodynamic Properties of the Elements"; American Society for Metals: Metals Park, OH, 1973.

16. Pearson, W. B. "A Handbook of Lattice Spacings and Structures of Metals and Alloys"; Pergamon: New York, 1967; Vol. 2, p. 480.

17. Julien-Pouzol, M.; Jaulmes, S.; Guittard, M.; Laruelle, P. J. Solid State Chem. 1978, 26, 185.

18. Dismukes, J. P.; White, J. G. Inorg. Chem. 1964, 3, 1220.

19. Myers, C. E.; Franzen, H. F.; Nguyen, T.-H. Ames Laboratory, Ames, IA, unpublished results.

20. Kim, K. S.; Winograd, N. Chem. Phys. Lett. 1975, 31, 312.

21. Frost, D. C.; McDowell, C. A.; Wallbank, B. Chem. Phys. Lett. 1976, 40, 189.

22. Vernon, G. A.; Stucky, G.; Carlson, T. A. Inorg. Chem. 1976, 15, 278.

23. Larsson, S. J. Electron Spectrosc. and Rel. Phenom. 1976, 8, 171.

24. Hagenmuller, D. Prog. Solid State Chem. 1971, 5, 71.

25. Kopp, L.; Harmon, B. N.; Liu, S. H. Solid State Commun. 1977, 22, 677.

26. Wolfram, T. Phys. Rev. Lett. 1972, 29, 1383.

27. Campagna, M.; Wertheim, G. K.; Shanks, H. R.; Zumsteg, F.; Banks, E. Phys. Rev. Lett. 1975, 34, 738.

28. Wertheim, G. K.; Campagna, M.; Chazalviel, J.-N.; Buchanan, D. N. E.; Shanks, H. R. Appl. Phys. 1977, 13, 225.

29. Chazaviel, J.-N.; Campagna, M.; Wertheim, G. K.; Shanks, H. R. Phys. Rev. B 1977, 16, 697.

SUMMARY AND DISCUSSION

A structural phase transition in $Sc_{0.81}S$ which is the result of partial vacancy ordering at low temperatures ($R\bar{3}m$) and random vacancy distribution at high temperatures ($Fm3m$), was found to occur at 700°C. This transition was used to test the hypothesis that vacancy ordering is driven by electrostatic interactions. However, the ionic model failed to predict the observed long range ordering in a number of ways and predicted a short range ordering which is not observed. On this basis, it is concluded that vacancy ordering in $Sc_{0.81}S$ is not the result of electrostatic interactions. It might also be suggested that the ionic model, because of its simplicity, has been over-extended in this and other cases.

A more realistic approach to analyzing bonding interactions is through quantum mechanical band calculations. The band structure results of ScS are interpreted as follows: the ℓ-character of the wavefunctions (ψ) which describe states in the valence and conduction bands and the directional nature of the electron density ($\psi^*\psi$) imply considerable nonmetal-metal σ-type bonding (S 2p - Sc $3de_g$) within the valence band states, i.e., the covalent bonding component, and primarily metal-metal σ-bonding (Sc 3d t_{2g} states) and to a lesser extent, nonmetal-metal π-bonding

(S 2p - Sc 3d t_{2g}) within the conduction band states. Similar bonding interpretations apply to other NaCl-type transition metal compounds as well, i.e., the NaCl structure does not prohibit covalent and metallic interactions.

The XPS results predict significant covalent character in the bonding in ScS, as evidenced by the small binding energy shifts noted for both scandium and sulfur relative to the pure elements. This is in support of the band structure predictions. Also, the theoretical valence density of states is in general agreement with the UPS spectrum of ScS. Finally, the ~12 kcal thermodynamic stability of ScP (8 valence electrons) over ScS (9 valence electrons) in a rigid band interpretation, implies that the additional electron in ScS occupies a slightly antibonding state, consistent with the view that the mixing of p-d states forms bonding (valence) and antibonding (conduction) bands.

It was previously stated that a study of the scandium-sulfur system served to link the chemistry of the typical ionic solids formed by the alkali and alkaline earth metals with the chemistry of the covalent and metallic transition metal compounds. Indeed, scandium monosulfide adopts the NaCl-type structure, a prototype ionic structure, but it has been shown that this compound is not an ionic solid. Rather, the metal d orbitals, even of this $3d^1$ metal Sc, promote covalent nonmetal-metal σ-type interactions, as well as metal-metal σ and nonmetal-metal π bonding interactions.

SUGGESTIONS FOR FUTURE RESEARCH

Several projects may be suggested as extensions of the research reported in this dissertation, some of which are already in progress. First of all, a self-consistent field band structure calculation should be completed for ScS. These results would be expected to agree more closely with the observed UPS spectrum than the results reported here. It would also be interesting, although more complicated, to pursue the effect of defects on the band structure to test the validity of the rigid bond model for $Sc_{1-x}S$ and to observe band structure changes which occur as a result of vacancy ordering, e.g., $R\bar{3}m$ to $Fm3m$ in $Sc_{0.8}S$.

The interesting parallels found for Na_xWO_3 and $Sc_{1-x}S$ could be pursued. Specifically, a thorough investigation of changes in the optical properties with composition should be attempted. Results of optical measurements combined with joint density of state, i.e., density of direct transitions E_i to E_f as a function of E_f-E_i, calculations from the ScS band structure may reveal the color mechanism in $Sc_{1-x}S$, especially if related to a similar study on Na_xWO_3 (11).

Finally, it would be of thermodynamic interest to measure the atomization enthalpy of ScSe (NaCl structure type (12)) since atomization enthalpies are known for ScP and ScS. In a preliminary vaporization study, stoichiometric

ScSe (a_c = 5) was repeatedly heated in vacuum at above 1600°C. The residue, in each case, showed weak superstructure lines in the powder pattern of the quenched material which could be indexed on the basis of a $R\bar{3}m$ cell similar to that observed for $Sc_{0.8}S$. The composition was not determined. The reported congruent composition is Sc_2Se_3 (12); however, a $R\bar{3}m$ superstructure has not been reported previously. This would warrant further study.

GENERAL REFERENCES

1. Jellinek, F. "MTP Int. Rev. Sci., Inorg. Chem."; Sharp, D. W. A., Ed.; Butterworths: London, 1972; Ser. 1, Vol. 5.

2. Rao, C. N. R.; Pisharody, K. P. R. Prog. Solid State Chem. 1976, 10, 207.

3. Bennett, L. H.; McAlister, A. J.; Watson, R. E. Physics Today 1977, 30, 34.

4. Franzen, H. F. Prog. Solid State Chem. 1978, 12, 1.

5. Dismukes, J. P.; White, J. G. Inorg. Chem. 1964, 3, 1220.

6. Tuenge, R. T. Ph.D. Dissertation, Iowa State University, Ames, IA, 1975.

7. Dismukes, J. P. J. Phys. Chem. Solids 1971, 32, 1689.

8. Narayan, P. B. V.; Finnemore, D. K. J. Less-Common Metals 1978, 61, 231.

9. Moodenbaugh, A. R.; Johnston, D. C.; Viswanathan, R. Mat. Res. Bull. 1974, 9, 1671.

10. Tuenge, R. T.; Laabs, F.; Franzen, H. F. J. Chem. Phys. 1976, 65, 2400.

11. Owen, J. F.; Teegarden, K. J.; Shanks, H. R. Phys. Rev. B 1978, 18, 3827.

12. Brozek, V.; Flahaut, J.; Guittard, M.; Julien-Pouzol, M.; Pardo, M.-P. Bull. Soc. Chim. Fr. 1974, 9/10, 1740.

ACKNOWLEDGEMENTS

The author wishes to express her sincere gratitude for the guidance and enthusiastic support received from Dr. H. F. Franzen during the course of this research. The technical expertise of and many helpful discussions with Jim Anderegg and Dr. A. V. Hariharan as well as the other group members were also much appreciated.

Thanks also to Sue Musselman for typing this manuscript.

To the roommates (past and present), friends, and especially Dad, Mom, Nan, John, Vince and Holly -- thank you for your patience, support and encouragement these past five years.

APPENDIX. PALS (POTENTIAL AT A LATTICE SITE): A PROGRAM TO CALCULATE LATTICE SITE POTENTIALS FOR ANY GIVEN CRYSTAL TYPE

Input for PALS

Card 1: Title card

columns: 1-80 title

Card 2: Lattice parameters and three program parameters

columns:

- 1-10: a (angstroms)
- 11-20: b (angstroms)
- 21-30: c (angstroms)
- 31-40: α (degrees)
- 41-50: β (degrees)
- 51-60: γ (degrees)

} real numbers to be punched anywhere in allowed columns with decimal point included

- 61-63: number of elements in compound
- 64-66: number of shells considered beyond the unit cell
- 67-69: one of the following integers depending of the value of $G(=\frac{1}{\eta})$
  1. small unit cell (lattice parameters <5.Å)
  2. large unit cell (lattice parameter ∿10)
  3. read in own value for G

} integers to be punched right - justified with no decimal point

70-72: number of formula units per unit cell

There will be a set of cards # 3,4,5 for each element -

Card 3: identifies element, number of symmetrically non-equivalent atoms, and number of symmetry operations

columns 1-2: ELEMENT symbol (2 letters)

3-4: number of non-equivalent sites

5-6: number of symmetry cards to be read in (including the identity operation)

integers which are right justified

Note: If there are several atoms which all are reproduced in the unit cell by the same set of symmetry cards, then include the symmetry cards for the first atom and for all others let number of symmetry operations = 0.

Card 4: These cards input the symmetry operations as follows. There is one card per operation and the identity operation must be included.

columns: 1-11 translation in the x_j coordinate

12-13 an integer +1, +2, +3, $-\underline{1}$, $-\underline{2}$, -3, which stands for x,y,z, $\bar{x}$,$\bar{y}$,$\bar{z}$ depending on how the x coordinate transforms

14-15 an integer ±1, ±2, ±3, or blank, is same as column 12-13 and used only in cases where x coordinate transforms into a linear combination of x,y,z, $\bar{x}$,$\bar{y}$,$\bar{z}$ or blank when not needed

16-26 translation in y_j coordinate

27-28 transformation of y_j coordinate

28-30 transformation of y_j coordinate

31-41 translation of z_j coordinate

42-43 transformation of z_j coordinate

44-45 transformation of z_j coordinate

The translation is a real number with decimal point included anywhere in specified region. The transformation are integer, right - justified, with the sign included in case of $\bar{x},\bar{y},\bar{z}$.

Card 5: Atomic position coordinates and associated charges. There is one card per nonequivalent atom.

columns: 1-10 x, 11-20 y, 21-30 z } fractional coordinates including decimal point anywhere in region

31-40 charge as it multiplies e } include decimal point and sign for anions.

Card 6: Only if reading in a value for G.

columns: 1-10 G (real number including decimal)

Note: Several sets of data may be processed at the same time. Two blank cards at the end of the data cards indicate the end of the program.

Output for PALS

I. x,y,z positions generated by symmetry are printed out such that all coordinates are between + and -0.5. The site number relates all symmetrically equivalent atoms and q is the charge of the ion at that site.

II. Site Number

Indicates which site potential is being calculated. A new list of anion and cation positions is generated with the site under consideration at the origin and all other ions within +0.5 and -0.5.

Shell Number identifies a particular region outward from the origin in both the direct and the reciprocal lattice.

Reciprocal Space identifies the contribution from the first summation in equation (1). The value of the constand term $(-2\zeta_p'/\pi^{\frac{1}{2}}\eta)$ in equation (1) is given in the output under the heading of the reciprocal space contribution for shell 1 (designated by *), since the latter is zero for shell 1.

Real Space identifies the contribution of the second summation in equation (1).

V SHELL refers to the sum of reciprocal space contribution + real contribution (i.e., the contribution to the total potential from that shell). This includes the constant term (see above).

Lattice Site Potential $= \sum_{\text{shells}} V_{\text{shell}}$.

For reliable LSP's, the reciprocal space terms and real space terms should both be converging and at similar rates. If not, choose another value for G. If the reciprocal term is not converging, choose G smaller. If the real term is not converging, choose G larger.

Madelung Energy refers to U_o as defined on page 14.

```
      DIMENSION TITLE(20),INDX(1000),X(100),Y(100),Z(100)
      DIMENSION NAME(5),NATM(10),NSYM(48),TR(3,48),MAT(3,2)
      DIMENSION XYZ(3,10),RQ(10),LS(100),Q(100),RXYZ(3)
      INTEGER R(3,3,48)
      COMMON/HKL/IH,K,L
      COMMON/HKLBAR/IHH(8),KK(8),LL(8),MM
C
C     ***************************************************************
C     * THIS PROGRAM CALCULATES LATTICE SITE POTENTIAL USING        *
C     * EWALD'S METHOD TO EVALUATE THE INFINITE SUM.  SEE           *
C     * TOSI, SOLID STATE PHYS, VOL.16(1964) 1.  ALSO LAB           *
C     * NOTEBOOK 1:37-42.....JEAN MERRICK...FALL 1976.....         *
C     * CARD 1:  TITLE                                              *
C     * CARD 2:                                                     *
C     * CELL PARAMETERS:A,B,C(ANGSTROMS),ALPHA,BETA,GAMMA(DEG)     *
C     *      (6F10.0)                                               *
C     * NELEM=NO. ELEMENTS IN COMPOUND  (I3)                        *
C     * LINDX=NO. SHELLS IN ADDITION TO UNIT CELL                   *
C     * IGOPT: OPTION FOR CALCULATION OF G  (I3)                    *
C     *      =1; G=SQRT(PI)/CAT-AN DISTANCE (SMALL UNIT CELL)       *
C     *      =2; LARGE UNIT CELLS (VAN GOOL)                        *
C     *      =3; READ G                                             *
C     * NFU=NO. FORMULA UNITS/UNIT CELL      (I3)                   *
C     ***************************************************************
C
  650 READ(5,600)(TITLE(I),I=1,20)
      READ(5,610)A,B,C,ALPHAI,BETAI,GAMMAI,NELEM,LINDX,IGOPT,
     1NFU
      IF(A.EQ.0.0)GO TO 1000
  600 FORMAT(20A4)
  610 FORMAT(6F10.0,4I3)
      WRITE(6,605)(TITLE(I),I=1,20)
      WRITE(6,505)
  605 FORMAT('1',20A4)
  505 FORMAT('0','*********************************************'
     1,'********************'/)
      ALPHA=ALPHAI/57.29578
      BETA=BETAI/57.29578
      GAMMA=GAMMAI/57.29578
      CALP=COS(ALPHA)
      CBET=COS(BETA)
      CGAM=COS(GAMMA)
      SALP=SIN(ALPHA)
      SBET=SIN(BETA)
      SGAM=SIN(GAMMA)
      VOL=A*B*C*(1.+2.*CALP*CBET*CGAM-CALP**2-CBET**2-CGAM**2)
     1**.5
      ARCP=B*C*SALP/VOL
      BRCP=A*C*SBET/VOL
      CRCP=A*B*SGAM/VOL
```

```
      CAR=(CBET*CGAM-CALP)/(SBET*SGAM)
      CBR=(CALP*CGAM-CBET)/(SALP*SGAM)
      CGR=(CALP*CBET-CGAM)/(SALP*SBET)
      AC=A*C*CBET
      AB=A*B*CGAM
      BC=B*C*CALP
      ABR=ARCP*BRCP*CGR
      ACR=ARCP*CRCP*CBR
      BCR=BRCP*CRCP*CAR
      WRITE(6,615)A,ALPHAI,B,BETAI,C,GAMMAI,VOL,LINDX,NELEM
  615 FORMAT('0','LATTICE PARAMETERS:',1X,'A=',F10.6,10X,'ALP'
     1,'HA=',F10.6/21X,'B=',F10.6,10X,'BETA =',F10.6/21X,'C=',
     2F10.6,10X,'GAMMA=',F10.6/1X,'CELL VOLUME=',F10.6/1X,'LA'
     3,'RGEST INDEX=',I5/1X,'ELEMENTS PER MOLECULE ',I5/)
C
C    ***************************************************************
C    * CARD 3:                                                     *
C    * NAME=ELEMENT NAME  (A2)                                     *
C    * NATM=NO. NON-EQUIV ATOMS OF THAT ELEMENT   (I2)             *
C    * NSYM=NO. SYMMETRY OPERATIONS  (I2)                          *
C    * CARD 4:                                                     *
C    * TR AND MAT REFER TO SYMMETRY OPERATION MATRICES             *
C    *      3(F11.6,2I2)                                          *
C    * CARD 5:                                                     *
C    * XYZ(I) ARE ATOMIC POSITION COORD.  3(F10.0)                 *
C    * RQ=CHARGE ON ION  (F10.0)                                   *
C    * REPEAT 3,4,5 FOR OTHER ELEMENTS                             *
C    ***************************************************************
C
C      GENERATES TRANS AND ROT MATRICES FROM SYMM OPERATIONS
C      READ IN
C
      NONEQ=0
      MCNT=0
      IEND=0
      DO 2000 II=1,NELEM
      READ(5,1010)NAME(II),NATM(II),NSYM(II)
 1010 FORMAT(A2,2I2)
      WRITE(6,1015)NAME(II),NATM(II),NSYM(II)
 1015 FORMAT('0','ATOM ',A2/1X,'NON EQUIVALENT ATOMS',I3/1
     1X,'SYMMETRY OPERATIONS',I3//)
      IEND=IEND+NATM(II)
      IF(NSYM(II).EQ.0)GO TO 1250
      ND=NSYM(II)
      DO 1100 I=1,ND
      READ(5,1110)(TR(K,I),(MAT(K,J),J=1,2),K=1,3)
 1110 FORMAT(3(F11.6,2I2))
      DO 1150 IL=1,3
      DO 1150 JJ=1,3
 1150 R(IL,JJ,I)=0.0
      DO 1100 J=1,3
```

```
      DO 1100 K=1,2
      IF(MAT(J,K).EQ.0)GO TO 1100
      ME=MAT(J,K)
      IM=IABS(ME)
      IS=ISIGN(1,ME)
      R(IM,J,I)=R(IM,J,I)+IS
 1100 CONTINUE
C     PRINTS ROT AND TRANS MATRICES
      WRITE(6,1025)
 1025 FORMAT(1X,'ROTATION AND TRANSLATION MATRICES'//)
      DO 1200 K=1,ND
      WRITE(6,1205)K,((R(I,J,K),I=1,3),TR(J,K),J=1,3)
 1205 FORMAT(1X,'SYMMETRY OPERATION',I3/3(1X,3I6,10X,F8.5/))
 1200 CONTINUE
      GO TO 1260
 1250 WRITE(6,1255)
 1255 FORMAT(1X,'MATRICES THE SAME AS ABOVE'/)
 1260 NA=NATM(II)
      WRITE(6,1275)
 1275 FORMAT('0',11X,'X',12X,'Y',12X,'Z',12X,'Q',6X,'SITE'//)
      DO 2000 L=1,NA
      NONEQ=NONEQ+1
C
C     READS ALL NON EQUIV POSITIONS AND GENERATES SYMM RELATED
C     POSITIONS
C
      READ(5,1305)(XYZ(MM,L),MM=1,3),RQ(L)
 1305 FORMAT(4F10.0)
      RAC=0.0
      DO 1270 NN=1,3
      IF(XYZ(NN,L).LT.(-0.5))XYZ(NN,L)=XYZ(NN,L)+1.
      IF(XYZ(NN,L).GT.0.5)XYZ(NN,L)=XYZ(NN,L)-1.
 1270 CONTINUE
      DO 2000 I=1,ND
      DO 1500 J=1,3
      R1=R(1,J,I)
      R2=R(2,J,I)
      R3=R(3,J,I)
      RXYZ(J)=XYZ(1,L)*R1+XYZ(2,L)*R2+XYZ(3,L)*R3+TR(J,I)
      IF(RXYZ(J).LT.(-0.5))RXYZ(J)=RXYZ(J)+1.
      IF(RXYZ(J).GT.0.5)RXYZ(J)=RXYZ(J)-1.
 1500 CONTINUE
      MCNT=MCNT+1
      X(MCNT)=RXYZ(1)
      Y(MCNT)=RXYZ(2)
      Z(MCNT)=RXYZ(3)
      Q(MCNT)=RQ(L)
      LS(MCNT)=NONEQ
C     MCNT LABELS EACH SITE IN UNIT CELL
C     LS LABELS ONLY NON EQUIV SITES
      WRITE(6,1405)MCNT,X(MCNT),Y(MCNT),Z(MCNT),Q(MCNT),
```

```
     1LS(MCNT)
 1405 FORMAT(1X,I2,4F13.6,I6)
 2000 CONTINUE
      NSITE=MCNT
      DO 150 K=1,NSITE
      IF(Q(K).EQ.Q(1))GO TO 150
      DX=X(K)-X(1)
      DY=Y(K)-Y(1)
      DZ=Z(K)-Z(1)
      RNO=2.*(DX*DY*AB+DX*DZ*AC+DY*DZ*BC)
      RACI=SQRT((DX*A)**2+(DY*B)**2+(DZ*C)**2+RNO)
      IF(RACI.LT.RAC.OR.RAC.EQ.0.0)RAC=RACI
  150 CONTINUE
C     CALCULATES VALUE FOR G
      GO TO (705,715,725),IGOPT
  705 G=1.77245381/RAC
      GO TO 700
  715 AP=VOL/(B*C*SALP)
      BP=VOL/(A*C*SBET)
      CP=VOL/(A*B*SGAM)
      APP=AMIN1(ARCP,BRCP,CRCP)
      AM=AMIN1(AP,BP,CP)
      G=SQRT(3.1416*APP/AM)
      GO TO 700
  725 READ(5,610)G
  700 WRITE(6,750)G,NFU
  750 FORMAT('0','THE CONSTANT G',F9.5/1X,'FORMULA UNITS PER '
     1,'UNIT/CELL',I4//)
      MSITE=1
      UEV=0.0
    ) DO 114 M=1,NSITE
      IF(LS(M).NE.MSITE)GO TO 114
      WRITE(6,520)MSITE
      FORMAT('1','SITE NUMBER',I4//)

       SSUME ORIGIN OF CELL IS AT SITE UNDER CONSIDERATION AND
       ICATE OTHERS SUCH THAT COORD. ARE BETWEEN 0.5 AND -0.5

         X(M)
         Y(M)
          (M)
          M)
            120
           UE
             K=1,NSITE
            K)-XO
            K)-YO
             )-ZO
              GT.0.5)X(K)=X(K)-1.
               T.0.5)Y(K)=Y(K)-1.
               T.0.5)Z(K)=Z(K)-1.
```

```
      IF(X(K).LT.(-0.5))X(K)=X(K)+1.
      IF(Y(K).LT.(-0.5))Y(K)=Y(K)+1.
      IF(Z(K).LT.(-0.5))Z(K)=Z(K)+1.
  124 CONTINUE
      WRITE(6,645)
  645 FORMAT(1X,'THE CATION POSITIONS AND CHARGES:',35X,'THE '
     1,'ANION POSITIONS AND CHARGES ARE:'/)
      SUMO=0.0
      DO 855 I=1,NSITE
      IF(Q(I))830,820,820
  820 WRITE(6,825)X(I),Y(I),Z(I),Q(I)
  825 FORMAT(1X,4F12.6)
      GO TO 855
  830 WRITE(6,835)X(I),Y(I),Z(I),Q(I)
  835 FORMAT(69X,4F12.6)
  855 CONTINUE
C     CALCULATES CONTRIBUTION TO LSP FROM SHELL 1
      LINDX=LINDX+1
      NO=0
      DO 799 I=1,LINDX
      IH=I-1
      DO 799 J=1,LINDX
      K=J-1
      DO 799 M=1,LINDX
      L=M-1
      NO=NO+1
      INDX(NO)=IH*10**6+K*10**3+L
  799 CONTINUE
      WRITE(6,205)
  205 FORMAT('0',2X,'SHELL',7X,'RECIPROCAL',11X,'REAL',15X,
     1'V SHELL'/3X,'NUMBER',8X,'SPACE',14X,'SPACE'//)
      DO 899 I=1,NSITE
      IF(X(I).EQ.0.0.AND.Y(I).EQ.0.0.AND.Z(I).EQ.0.0)GO TO 899
      DRA=2.*(AB*X(I)*Y(I)+AC*X(I)*Z(I)+BC*Y(I)*Z(I))
      DR=SQRT((X(I)*A)**2+(Y(I)*B)**2+(Z(I)*C)**2+DRA)
      TERMO=Q(I)*ERFC(G*DR)/DR
      SUMO=SUMO+TERMO
  899 CONTINUE
      T=(-1.12838)*G*QP
      PLSO=SUMO+T
      WRITE(6,655)T,SUMO,PLSO
  655 FORMAT(5X,'1',8X,E13.6,'*',4X,2(E13.6,5X))
C     CALCULATES CONTRIBUTION TO LSP FROM OTHER SHELLS
      PLS=0.0
      DO 299 NSHLL=2,LINDX
      MAXH=NSHLL-1
      RCPI=0.0
      REALI=0.0
      VSHELL=0.0
      DO 399 MSRT=1,NO
      IH=INDX(MSRT)/10**6
```

```
      K=(INDX(MSRT)-IH*10**6)/10**3
      L=INDX(MSRT)-(IH*10**6)-(K*10**3)
      IF(MAX0(IH,K,L).NE.MAXH)GO TO 399
      CALL SIGNS
      DO 499 ISIG=1,MM
      RH=IHH(ISIG)
      RK=KK(ISIG)
      RL=LL(ISIG)
      HSQA=2.*(RH*RK*ABR+RH*RL*ACR+RK*RL*BCR)
      HSQ=39.478416*((RH*ARCP)**2+(RK*BRCP)**2+(RL*CRCP)**2+HS
     1QA)
      TRCP=0.0
      TREAL=0.0
      DO 599 J=1,NSITE
      XH=RH-X(J)
      YK=RK-Y(J)
      ZL=RL-Z(J)
      DLR=SQRT((XH*A)**2+(YK*B)**2+(ZL*C)**2+2.*(XH*YK*AB+XH*Z
     1L*AC+YK*ZL*BC))
      HDOTR=6.2831852*(RH*X(J)+RK*Y(J)+RL*Z(J))
      SRCP=Q(J)*COS(HDOTR)
      GDLR=G*DLR
      IF(GDLR.LT.10.)GO TO 551
      SREAL=0.0
      GO TO 555
551   SREAL=Q(J)*ERFC(GDLR)/DLR
555   TRCP=TRCP+SRCP
      TREAL=TREAL+SREAL
599   CONTINUE
      HSQG=HSQ/(4.*G**2)
      IF(HSQG.LT.100)GO TO 420
      TTRCP=0.0
      GO TO 430
420   TTRCP=12.56637*TRCP*EXP(-HSQG)/(VOL*HSQ)
430   VHKL=TTRCP+TREAL
      RCPI=RCPI+TTRCP
      REALI=REALI+TREAL
      VSHELL=VSHELL+VHKL
499   CONTINUE
      IF(IH.EQ.K.AND.IH.EQ.L)GO TO 200
399   CONTINUE
200   WRITE(6,300)NSHLL,RCPI,REALI,VSHELL
300   FORMAT(4X,I2,8X,3(E13.6,5X))
      PLS=PLS+VSHELL
299   CONTINUE
      PLSTOT=PLS+PLSO
      PLSEV=14.400701*PLSTOT
      PLSKCL=PLSEV*23.062
      WRITE(6,303)
303   FORMAT(1X,'* THIS TERM = -2GQ(0)/SQRT(PI)')
      WRITE(6,910)PLSTOT,PLSEV,PLSKCL
```

```
  910 FORMAT('0','LATTICE SITE POTENTIAL = ',E13.6,' /ANGSTRO'
     1,'M'/24X,'= ',E13.6,' EV'/24X,'= ',E13.6,' KCAL/MOLE')
      FUNTS=NFU
      FREQ=0.0
C     CALCULATION OF MADELUNG ENERGY
      DO 915 IJ=1,MCNT
      IF(LS(IJ).NE.MSITE)GO TO 915
      FREQ=FREQ+1.
      CHARG=Q(IJ)
  915 CONTINUE
      UEV=UEV+FREQ*CHARG*PLSEV/(2.*FUNTS)
C     CALCULATIONS REPEATED FOR ALL NON EQUIV POSITIONS
      IF(MSITE.EQ.IEND)GO TO 920
      MSITE=MSITE+1
      LINDX=LINDX-1
      GO TO 500
  920 UKCAL=23.062*UEV
      WRITE(6,930)UEV,UKCAL
  930 FORMAT('0','MADELUNG ENERGY FOR THE CRYSTAL IS ',E13.6,
     1 ' EV'/36X,E13.6,' KCAL/MOLE')
      GO TO 650
 1000 STOP
      END
      SUBROUTINE SIGNS
C
C     THIS DETERMINES ALL SIGN PERMUTATIONS OF THE TRIPLE READ
C     IN
C
      COMMON/HKL/IH,K,L
      COMMON/HKLBAR/IHH(8),KK(8),LL(8),MM
      IF(IH.NE.0.AND.K.NE.0.AND.L.NE.0)GO TO 103
      IF(IH.EQ.0.AND.K.EQ.0)GO TO 203
      IF(IH.EQ.0.AND.L.EQ.0)GO TO 303
      IF(K.EQ.0.AND.L.EQ.0)GO TO 403
      IF(IH.EQ.0)GO TO 503
      IF(K.EQ.0)GO TO 603
      DO 703 I=1,2
      IHH(I)=IH
  703 LL(I)=L
      DO 713 I=3,4
      IHH(I)=-IH
  713 LL(I)=L
      KK(1)=K
      KK(2)=-K
      KK(3)=K
      KK(4)=-K
      MM=4
      GO TO 63
  603 DO 613 I=1,2
      IHH(I)=IH
  613 KK(I)=K
```

```
      DO 623 I=3,4
      IHH(I)=-IH
  623 KK(I)=K
      LL(1)=L
      LL(2)=-L
      LL(3)=L
      LL(4)=-L
      MM=4
      GO TO 63
  503 DO 513 I=1,2
      IHH(I)=IH
  513 KK(I)=K
      DO 523 I=3,4
      IHH(I)=IH
  523 KK(I)=-K
      LL(1)=L
      LL(2)=-L
      LL(3)=L
      LL(4)=-L
      MM=4
      GO TO 63
  403 DO 413 I=1,2
      KK(I)=K
  413 LL(I)=L
      IHH(1)=IH
      IHH(2)=-IH
      MM=2
      GO TO 63
  303 DO 313 I=1,2
      IHH(I)=IH
  313 LL(I)=L
      KK(1)=K
      KK(2)=-K
      MM=2
      GO TO 63
  203 DO 213 I=1,2
      IHH(I)=IH
  213 KK(I)=K
      LL(1)=L
      LL(2)=-L
      MM=2
      GO TO 63
  103 DO 13 I=1,4
   13 IHH(I)=IH
      DO 23 I=5,8
   23 IHH(I)=-IH
      DO 33 I=1,8
      GO TO (1,1,2,2,1,1,2,2),I
    1 KK(I)=K
      GO TO 33
    2 KK(I)=-K
```

```
   33 CONTINUE
      DO 53 I=1,7,2
      J=I+1
      LL(I)=L
   53 LL(J)=-L
      MM=8
   63 RETURN
      END
```

```
SCS  FCC
*****************************************************************

LATTICE PARAMETERS: A=   5.165000          ALPHA= 90.000000
                    B=   5.165000          BETA = 90.000000
                    C=   5.165000          GAMMA= 90.000000
CELL VOLUME=137.787811
LARGEST INDEX=     4
ELEMENTS PER MOLECULE      2

ATOM SC
NON EQUIVALENT ATOMS  1
SYMMETRY OPERATIONS  4


ROTATION AND TRANSLATION MATRICES


SYMMETRY OPERATION  1
     1      0      0            0.0
     0      1      0            0.0
     0      0      1            0.0

SYMMETRY OPERATION  2
     1      0      0            0.0
     0      1      0            0.50000
     0      0      1            0.50000

SYMMETRY OPERATION  3
     1      0      0            0.50000
     0      1      0            0.50000
     0      0      1            0.0

SYMMETRY OPERATION  4
     1      0      0            0.50000
     0      1      0            0.0
     0      0      1            0.50000
```

	X	Y	Z	Q	SITE
1	0.0	0.0	0.0	2.000000	1
2	0.0	0.500000	0.500000	2.000000	1
3	0.500000	0.500000	0.0	2.000000	1
4	0.500000	0.0	0.500000	2.000000	1

ATOM S
NON EQUIVALENT ATOMS 1
SYMMETRY OPERATIONS 0

MATRICES THE SAME AS ABOVE

	X	Y	Z	Q	SITE
5	0.500000	0.500000	0.500000	-2.000000	2
6	0.500000	0.0	0.0	-2.000000	2
7	0.0	0.0	0.500000	-2.000000	2
8	0.0	0.500000	0.0	-2.000000	2

THE CONSTANT G 0.68633
FORMULA UNITS PER UNIT/CELL 4

SITE NUMBER 1

SHELL NUMBER	RECIPROCAL SPACE	REAL SPACE	V SHELL
1	-0.154889E 01*	-0.276801E-01	-0.157657E 01
2	0.249223E 00	-0.264264E-01	0.222796E 00
3	0.0	-0.361038E-13	-0.361038E-13
4	0.381197E-03	-0.192103E-35	0.381197E-03
5	0.0	0.0	0.0

* THIS TERM = -2GQ(0)/SQRT(PI)
LATTICE SITE POTENTIAL = -0.135339E 01 /ANGSTROM
= -0.194897E 02 EV
= -0.449472E 03 KCAL/MOLE

SITE NUMBER 2

SHELL NUMBER	RECIPROCAL SPACE	REAL SPACE	V SHELL
1	0.154889E 01*	0.276800E-01	0.157657E 01
2	-0.249223E 00	0.264264E-01	-0.222796E 00
3	0.0	0.361038E-13	0.361038E-13
4	-0.381197E-03	0.192103E-35	-0.381197E-03
5	0.0	0.0	0.0

* THIS TERM = -2GQ(0)/SQRT(PI)

LATTICE SITE POTENTIAL = 0.135339E 01 /ANGSTROM
= 0.194897E 02 EV
= 0.449472E 03 KCAL/MOLE

MADELUNG ENERGY FOR THE CRYSTAL IS -0.389795E 02 EV
-0.898945E 03 KCAL/MOLE